JOURNAL OF
CHEMICAL INFORMATION
AND MODELING

Article

Acetylcholinesterase Inhibitors: Structure Based Design, Synthesis, Pharmacophore Modeling and Virtual Screening

Koteswara Rao Valasani, Michael O. Chaney, Victor W. Day, and Shirley ShiDu Yan

J. Chem. Inf. Model., **Just Accepted Manuscript** • DOI: 10.1021/ci400196z • Publication Date (Web): 18 Jun 2013

Journal of Chemical Information and Modeling is published by the American Chemical Society. 1155 Sixteenth Street N.W., Washington, DC 20036

Acetylcholinesterase Inhibitors: Structure Based Design, Synthesis, Pharmacophore Modeling and Virtual Screening

Koteswara Rao Valasani, Michael O. Chaney, Victor W. Day and Shirley ShiDu Yan*

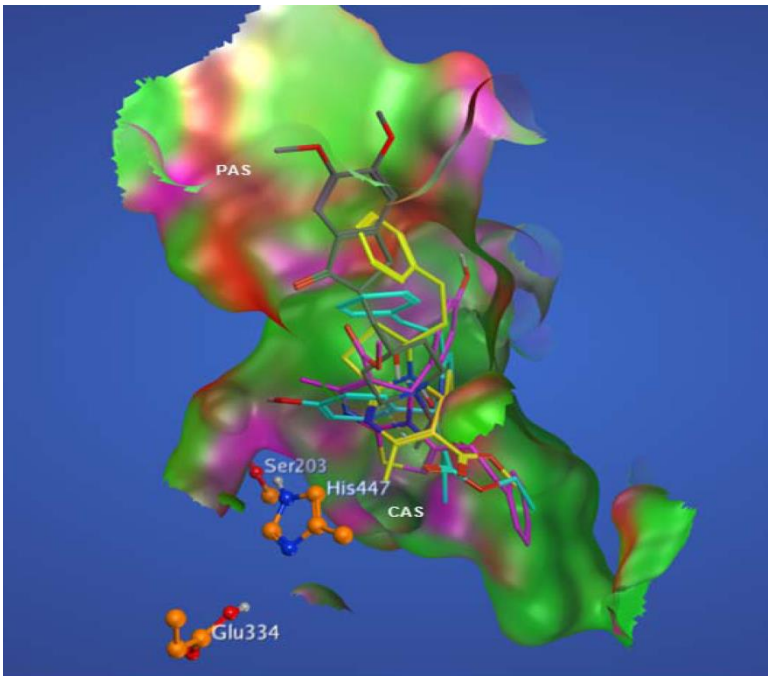

Acetylcholinesterase (AChE) is one of the main drug targets and its inhibitors have demonstrated functionality in the symptomatic treatment of Alzheimer's disease (AD). Structure based design has been used to identify the human AChE inhibitors. Both 2D QSAR and 3D pharmcophore models were created. AChE molecular docking studies were undertaken to determine whether they exhibit significant binding affinity with the binding site.

Acetylcholinesterase Inhibitors: Structure Based Design, Synthesis, Pharmacophore Modeling and Virtual Screening

Koteswara Rao Valasani[1], Michael O. Chaney[1], Victor W. Day[2], and Shirley ShiDu Yan[1]*

[1]Department of Pharmacology & Toxicology and Higuchi Bioscience Center, School of Pharmacy, University of Kansas, Lawrence, KS 66047 (USA)

[2]Department of Chemistry, University of Kansas, Lawrence, KS 66045 (USA)

*Correspondence should be addressed to Dr. Shirley Shidu Yan, 2099 Constant Avenue, University of Kansas, Lawrence, KS 66047. E-mail: shidu@ku.edu.

A B S T R A C T

Acetylcholinesterase (AChE) is one of the main drug targets and its inhibitors have demonstrated functionality in the symptomatic treatment of Alzheimer's disease (AD). In this study, a series of novel AChE inhibitors were designed and their inhibitory activity was evaluated with 2D QSAR studies using a training set of 20 known compounds for which IC_{50} values had previously been determined. The QSAR model was calculated based on 7 unique descriptors. Model validation was determined by predicting IC_{50} values for a test set of 20 independent compounds with measured IC_{50} values. A correlation analysis was carried out comparing the statistics of the measured IC_{50} values with predicted ones. These selectivity-determining descriptors were interpreted graphically in terms of principle component analyses (PCA). A 3D pharmacophore model was also created based on the activity of the training set. In addition, absorption, distribution, metabolism and excretion (ADME) descriptors were also determined to evaluate their pharmacokinetic properties. Finally, molecular docking of these novel molecules into the AChE binding domain indicated that three molecules (**6c**, **7c** and **7h)** should have significantly higher affinities and solvation energies than the known standard drug donepezil. The docking studies of 2*H*-thiazolo[3,2-a]pyrimidines (**6a**-**6j**) and 5*H*-thiazolo[3,2-a] pyrimidines (**7a**-**7j**) with human AChE have demonstrated that these ligands bind to the dual sites of the enzyme. Simple and ecofriendly syntheses and diastereomeric crystallizations of 2*H*-thiazolo [3,2-a]pyrimidines and 5*H*-thiazolo[3,2-a] pyrimidines are described. The solid-state structures for the HBr salts of compounds **6a, 6e, 7a and 7i** have been determined using single-crystal X-ray diffraction techniques and x-ray powder patterns were measured for the bulk solid

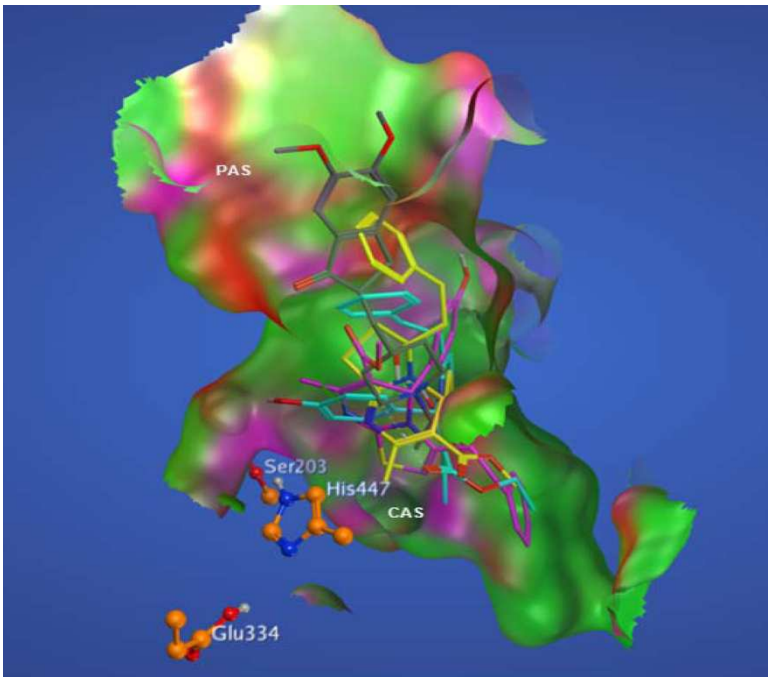

remaining after solvent was removed from solutions containing **6a** and **7a**. These studies provide valuable insight for designing more potent and selective inhibitors for the treatment of AD.

1. INTRODUCTION

Alzheimer's disease (AD) is the most common cause of dementia in adults, resulting in a disorder of cognition and memory due to neuronal stress and eventually in cell death. Alzheimer brain is characterized by two pathological features: amyloid beta (Aβ) accumulation and the formation of neurofibrillary tangles. Accumulation of Aβ is considered to be one of the primary causes for the AD pathogenesis. Scientists have proposed several hypotheses for AD development[1-9]. One of the oldest AD hypotheses, the cholinergic hypothesis [10], has led to the development of cholinesterase inhibitors (ChEIs) that increase levels of acetylcholine (ACh) through inhibition of cholinesterases (ChEs) [11]. The most predominant hypothesis, the amyloid hypothesis[12, 13] postulates that increased production of β-amyloid peptide and its aggregation and accumulation in a brain lead to neuronal cell death. Since it is known that ACh deficiency is associated with AD[14] , inhibiting the biological activity of ChEs to increase ACh levels in the brain is one of the major therapeutic strategies for the treatment of AD. Acetylcholinesterase (AChE) inhibitors are the most frequently prescribed drugs for AD, which promote memory function and delay the cognitive decline without altering the underlying pathology.

The deficiencies in cholinergic neurotransmission in AD have led to the development of potent AChE inhibitors (AChEIs). A large number of naturally-occurring and synthetic AChE inhibitors have already been identified[15, 16] as the first-line treatment for symptoms of this disease and are prescribed for mild-to-moderate AD. Four AChEIs have been approved by the United States FDA and many other jurisdictions for the treatment of AD[17-19]: tacrine, donepezil, rivastigmine, and galantamine. Tacrine is no longer in general use because of dosing, tolerability and safety concerns. The clinical benefits of these agents include improvements, stabilization or less-than-expected decline in cognition and other mental function. Slightly different mechanisms of action have been reported for the available inhibitors. They appear to affect the ease of use and tolerability more than drug effectiveness though, since neither systematic reviews, nor head-to-head studies, identify significant efficacy differences between the agents[20-22]. Subsequent

clearly-reported, carefully-conducted, systematic, evidence-based reviews of these agents are available[20, 23-25]. It is important to understand that none of these medications stop the disease itself. At best, they only slow progression and do not appear to affect the basic destructive disease process. When patients go off the drugs, the deterioration continues.

Although all of the FDA-approved Alzheimer's medicines have, in general, been shown to *somewhat* improve a patient's well-being, most patients will not experience *significant* improvement. Studies have shown that only about 10 percent of patients are considered to be "better" when assessed by their doctor or caregiver. The remaining 90% may not decline as much as they would have without drug treatment but overall *improvement* will likely not be noted. While head-to-head studies of the various medicines could provide meaningful comparisons for some aspects of AD treatment, it is difficult to make head-to-head comparisons in their ability to improve overall well-being.

The 3-D structure of AChE from native Torpedo californica (TcAChE) has been determined by X-ray crystallography (Protein Data Bank, PDB code: 2ACE)[26] and is similar to the structure of human AChE (*h*AChE). Both molecules are α/β serine hydrolases with 537 residues and a 12-stranded mixed β sheet surrounded by 14 α helices. The active sites in both crystal structures are also similar. Docking simulations were performed to gain insight into the recognition between the AChE and the ligands. For *Tc*AChE, these experiments indicated that recognition occurred in a deep, narrow groove approximately 20Å long on the enzyme surface. For TcAChE, this groove contains both the catalytic active site (CAS) with the Ser-His-Glu catalytic triad (Ser203-His447-Glu334) and the peripheral anionic site (PAS) that utilizes Trp86, Tyr133, Glu202, Phe338, and Tyr449. A substantial portion of the surface of this groove is lined by fourteen highly conserved aromatic residues. The PAS is located at the aromatic-lined entrance of the groove. This aromatic lined-entrance contains Tyr72, Tyr124, Trp279 and Tyr337 residues [27]. Reversible inhibitors bind to the CAS or to the PAS and dimeric (dual) inhibitors bind simultaneously to both of the sites. Non-catalytic roles of AChE have been established in the past decade. AChE has been shown to play a key role in the acceleration of amyloid β (Aβ)-peptide deposition and promoting the formation of amyloid β-plaques [27]. Dual-binding AChE inhibitors which bind to PAS have been shown to inhibit such processes [28]. A single molecule can therefore serve two important biological roles.

Further studies indicated that the hydrophobic environment close to the PAS promotes the interaction of AChE with Aβ-peptide to form Aβ fibrils that lead to neurotoxicity[29, 30]. These reports suggest that AChEIs enhance the release of non amyloidogenic soluble derivatives of amyloid precursor protein (APP) both *in vitro* and *in vivo*, thereby slowing the formation of amyloidogenic compounds in the brain.[31]. AChEIs also increase the solubility of APP.[32] Numerous clinical trials have revealed the safety and efficacy of AChEIs in the treatment of AD. Preclinical studies suggested that these AChEIs also attenuate neuronal cell death from neuronal cytotoxicity and therefore provide another treatment for AD.[33]

Since it was also discovered that AChE augments the neurotoxic effect of Aβ peptide by accelerating the formation of beta amyloid deposits in the brain, the role of Aβ peptide at the onset and during progression of AD is a matter of debate.[34, 35] It is well known that the enzyme interacts with beta amyloid through the PAS and promotes the formation of fibrils.[36] We have therefore focused on developing compounds that are able to interact with both the CAS and PAS of AChE as a potentially new therapeutic approach for the effective management of AD symptoms.[32, 37]

Pyrimidine derivatives are widely used as treatment of AD at different stages[38-41] and they have previously been reported to be useful as gamma secretase modulators,[42] treatments for diseases like AD associated with the deposition of beta-amyloid peptide in the brain [39], inhibitors for microtubule affinity regulating kinases [43] or compounds for the treatment or prevention of tauopathies [44].

Since pyrimidines are also components or building blocks for the synthesis of many important biologically active compounds[45, 46] and the groove of AChE is lined with a high percentage of aromatic side-chains, we concentrated on synthesizing molecules with aromatic side chains attached to a pyrimidine moiety. Herein, we report the design, molecular docking studies, QSAR studies, preADME predictions, 3D Pharmacophore modeling results, synthesis, diastereomeric crystallization, single crystal XRD and powder XRD for AChEIs of pyrimidine derivatives.

2. MATERIALS AND METHODS

Construction of a 2D QSAR model [47]

The QSAR suite of applications in MOE was used to calculate and analyze the data and build numerical models of the data for prediction and interpretation purposes. Any QSAR model for a given set of molecules correlates the activities with properties inherent to each molecule in the set itself. A database of 40 compounds with known IC_{50} values was used to generate independent training and test data sets. Initially, a total of 7 QSAR descriptors were defined for the training set compounds to carry out a correlation analysis and to construct the QSAR model based on these properties. These descriptors are all independent variables and the IC_{50} values of the each compound were considered as dependent variable to predict the activity of each test set compound.

Fitting the experimental data

The predicted activities were chosen as dependent variable in the test data set and a QSAR model was constructed choosing this predicted activity and the remaining descriptors as model fields. Regression analysis was performed for the training data set and Root Mean Square Error (RMSE) and r^2 values of the fit were reported. This fit model was saved as the QSAR model and used for the prediction of activities of compounds of test data set.

Cross-Validating the Model

The above QSAR fit was used for both model validation and cross validation. This validation procedure will evaluate the predicted activities and the residuals for the training set molecules. The predicted, residual and Z-score values were calculated for both model and cross validations.

Graphical Analysis

The predictive ability of the model was assessed using a correlation plot by plotting the predicted ($PRED) values (X-axis) versus the predicted IC_{50} activities (Y-axis). This correlation plot was used to identify outliers that have a Z-score beyond the range of 2.

Estimation and validation of predicted activities of test set

The QSAR model fit obtained above was used to evaluate the predicted (PRED Activity) values of 20 test set compounds. Regression analysis was performed for the test data set and Root Mean Square Error (RMSE) and r^2 values of the fit were reported.

Pruning the Descriptors

Pruning the descriptors is necessary to select the optimum set of molecules under consideration. 'QuaSAR-Contingency,'a statistical application in MOE was used to describe the best molecules in the data set. The results were analyzed using Principle Component Analysis (PCA) and the purpose of which is to reduce the dimensionality of set of molecular descriptors by linearly transforming the data or defying a property that would be important to drug design. A Three-dimensional scatter graphical plot was generated using the first three Principal Components (PCA1, PCA2 and PCA3).

ADMET prediction[48, 49]

Absorption, Distribution, Metabolism, Excretion, & Toxicity (ADMET) properties of the 20 novel compounds were calculated using the preADMET online server (http://preadmet.bmdrc.org/). The ADMET properties, human intestinal absorption, *in vitro* Caco-2 cell permeability, *in vitro* Maden Darby Canine Kidney (MDCK) cell permeability, *in vitro* plasma protein binding and *in vivo* blood brain barrier penetration were predicted using this program.

Molecular Docking[50, 51]

Preparation of AChE protein

The three-dimensional structure of AChE was retrieved from the Protein Data Bank (PDB:http://www.rcsb.org/pdb, PDB ID: 1B41) and loaded into the MOE software. All water molecules and hetereo atoms were removed and polar hydrogens were added. Protonation of the

3D structure was done for all the atoms in implicit solvated environment (Born solvation model) at a specified temperature of 300K, pH of 7 and with a salt concentration value of 0.1. A non-bonded cut off value of 10 - 12 A^o was applied to the Leonard-Jones terms. After the protonation, the complete structure was Energy minimized in MMFF94x force field at a gradient cut off value of 0.05. Molecular dynamics simulations were carried out at a constant temperature of 300 deg K for a heat time of 10 pico seconds. The total simulations were carried out for a total period of 10 nano seconds. The time step was considered as 0.001 and the temperature relaxation time was set to 0.2 pico seconds. The position, velocity and acceleration were saved every 0.5 pico seconds

Prediction of Binding site for Ligands

The binding site for docking of our ligand candidates was defined by the donepezil inhibitor obtained from the AChE crystal structure (PDB:http://www.rcsb.org/pdb, PDB ID: 1B41). The donepezil molecule was obtained from the AChE crystal structure (PDB:http://www.rcsb.org/pdb, PDB ID: 4EY7). It was positioned into the 1B41 structure by alignment and superposition of the two proteins. The docking routine within MOE allows the user to define a binding region from the donepezil molecule. In our case we used r </= 10 A^o.

Molecular Docking [52]

The ligand data base generated from the list of all novel ligand molecules was docked into the specified binding domain of the AChE receptor using alpha PMI (Principle Moments of Inertia) placement methodology where Poses are generated by aligning ligand conformations principal moments of inertia to a randomly generated subset of alpha spheres in the receptor site. Thirty docked conformations were generated for each ligand and ranked by alpha HB scoring function which is a linear combination of the geometric fit of the ligand to the binding site and hydrogen bonding effects. From all the receptor-ligand complexes, the conformation with the lowest docking score was chosen for the analysis[57]. The interaction of all ligand molecules in the binding domain cavity was analyzed from ligand interaction study of MOE.[5] The ligand-receptor complexes were analyzed by both London ΔG free energy approximations and interaction energies, ΔE.

Pharmacophore Model

A pharmacophore defines both features and locations of important binding interactions between a ligand and its receptor. Our pharmacophore model was constructed by overlapping the top 6 ligand candidates that calculated with the strongest binding affinity. The Unified scheme within MOE was used to define the features thought to be important for ligand binding. The locations of these features were determined by inspection of strong interactions of the ligands with the AChE receptor.

Chemistry

General

All reagents were commercially available and used without further purification. Melting points were determined in open capillary tubes on a Laboratory Devices Mel-Temp apparatus and are uncorrected. ^{1}H and ^{13}C NMR spectra were recorded in d_6-DMSO on a Bruker DRX-500 spectrometer operating at 500 MHz, and 125 MHz, respectively and calibrated to the solvent peak. Abbreviations used for the split patterns of proton NMR signals are: singlet (s), doublet (d), triplet (t), quartet (q), quintet (qui), multiplet (m) and broad signal (br). High-resolution mass spectrometry (HRMS) was recorded on a LCT Premier Spectrometer.

Synthesis of methyl 4-(4-hydroxy-3-(methoxycarbonyl) phenyl)-6-methyl-2-thioxo-1, 2, 3, 4-tetrahydropyrimidine-5-carboxylate (4e)

To a stirred solution of ethyl acetoacetate (1 mmol), methyl 5-formyl-2-hydroxybenzoate (1 mmol) and thiourea (1 mmol) in ethanol (10 mL) was refluxed in the presence of poly phosphoric acid (1 mmol %) for 8 h. The progress of the reaction was monitored by TLC (dichloromethane: ethyl acetate, 1:1 v/v). After completion of the reaction, the reaction mixture was cooled to room temperature, and it was poured into crushed ice (20 g) and formed the white solid. The solid was filtered under suction, washed with ice-cold water and then recrystallized from hot ethanol to afford the methyl 4-(4-hydroxy-3-(methoxycarbonyl) phenyl)-6-methyl-2-

thioxo-1, 2, 3, 4-tetrahydropyrimidine-5-carboxylate (**4e**), white crystals; yield: 87 %; mp: 211-213 °C; R $_f$ 0.32; (dichloromethane: ethyl acetate, 1:1 v/v). IR: 3344, 3238, 2974, 2883, 1924, 1714, 1668, 1568, 1527, 1348, 1253, 881, 736, 698 cm^{-1}; ^{1}H NMR (DMSO-d_6) δ 2.30 (*s*, 3H), 3.55 (s, 3H), 3.89 (s, 3H), 5.14 (d, *J* = 5.0 Hz, 1H), 6.98-7.00 (m, 1H), 7.33-7.35 (m, 1H), 7.64 (d, *J* = 5.0 Hz, 1H), 9.63-9.66 (m, 1H), 10.36-10.39 (m, 1H), 10.49 (s, 1H); ^{13}C NMR (DMSO-d_6) δ 13.9, 17.2, 51.1, 52.5, 53.2, 59.6, 100.1, 112.9, 117.8, 127.9, 133.6, 134.2, 145.4, 159.4, 165.5, 168.8, 173.9.

The same experimental procedure was adopted for the preparation of the remaining title compounds **4a-4j**

Ethyl 4-(4-hydroxy-3-(methoxycarbonyl) phenyl)-6-methyl-2-thioxo-1,2,3,4-tetrahydropyrimidine-5-carboxylate (4j)

White crystals, 84% yield; mp: 239-241 °C; R_f 0.30; (dichloromethane: ethyl acetate, 1:1 v/v). Yield: 82%; IR: 3330, 3236, 2927, 2883, 1924, 1714, 1668, 1568, 1525, 1346, 1253, 1091, 1051, 881, 738, 698 cm^{-1}; ^{1}H NMR (DMSO-d_6) δ 1.11 (t, 3H), 2.29 (*s*, 3H), 3.89 (*s*, 3H), 3.96-4.06 (m, 2H), 5.14 (d, *J* = 5.0 Hz, 1H), 6.99 (d, *J* = 10.0 Hz, 1H), 67.34 (m, 1H), 7.65 (d, 1H), 9.63-9.64 (m, 1H), 10.36 (d, 1H), 10.48 (s, 1H); ^{13}C NMR (DMSO-d_6) δ 13.9, 17.1, 52.5, 53.3, 59.6, 100.4, 112.8, 117.9, 127.9, 133.6, 134.6, 145.1, 159.3, 164.9, 168.8, 173.9. HRMS cald for $C_{16}H_{18}N_2O_5S$ (M+H) 350.0936; found 453.0900 (TOF MS ES^+).

Synthesis of ethyl 3-hydroxy-7-methyl-5-(3-nitrophenyl)-3-phenethyl-3, 5-dihydro-2H-thiazolo [3, 2-a] pyrimidine-6-carboxylate (6a)

To a solution of ethyl 6-methyl-4-(3-nitrophenyl)-2-thioxo-1,2,3,4-tetrahydropyrimidine-5-carboxylate (4a) (1 mmol) in water (5 mL), and tetrahydrofuran (2.5 mL) and 1-bromo-4-phenylbutan-2-one (1 mmol) was added to this solution, and the reaction mixture was stirred for 8 h at room temperature. The progress of the reaction was monitored by TLC (dichloromethane: ethylacetate1:1). After completion of the reaction, white solid was formed. The solid was filtered off and washed with water and dried. The solid was recrystallized from methanol to get the pure product of ethyl 3-hydroxy-5-(4-hydroxy-3-(methoxycarbonyl) phenyl)-7-methyl-3-phenethyl-3,5-dihydro-2H-thiazolo[3,2-a]pyrimidine-6-carboxylate (**6a**). Color less solid, R_f 0.37; (dichloromethane: ethyl acetate, 1:1 v/v). Yield: 83%; m.p.: 217-220 ºC; IR: 3232, 2902, 2864,

2690, 2362, 1712, 1666, 1569, 1529, 1350, 1259, 1091, 748, 703 cm-1; ^{1}H NMR (DMSO-d$_6$) δ 1.18 (t, 3H), 2.27 (*s*, 3H), 2.39 (s, 2H), 2.67-2.85 (m, 2H), 3.54-3.58 (m, 1H), 3.96-4.19 (m, 3H), 5.80 (s, 1H), 6.922-6.95 (m, 1H), 7.12-7.32 (m, 5H), 7.64-7.70 (m, 1H), 7.78-7.89 (m, 1H), 8.14-8.20 (m, 2H); ^{13}C NMR (DMSO-d$_6$) δ 13.8, 17.7, 28.9, 36.8, 37.7, 48.6, 54.3, 54.8, 60.7, 105.1, 122.3, 123.2, 123.7, 126.2, 127.7, 128.2, 128.4, 130.7, 140.0, 143.8, 147.4, 147.6, 163.4, 166.6. HRMS cald for $C_{24}H_{26}N_3O_5S$ (M+H) 468.1593; found 468.1574 (TOF MS ES$^+$).

The same experiment procedure was followed for the remaining title compounds **6b-6j.**

Synthesis of ethyl 7-methyl-5-(3-nitrophenyl)-3-phenethyl-5H-thiazolo [3, 2-a] pyrimidine-6-carboxylate (7a)

Ethyl 3-hydroxy-7-methyl-5-(3-nitrophenyl)-3-phenethyl-3, 5-dihydro-2H-thiazolo [3, 2-a] pyrimidine-6-carboxylate (1mmol) in water (5 mL), and ethanol (3 mL) was taken in a reaction flux and refluxed for 6h. The progress of the reaction was monitored by TLC (dichloromethane: ethylacetate1:1). After completion of the reaction, the solvent was removed under reduced pressure. The solid was recrystallized from methanol to afforded the title compound methyl 7-methyl-5-(3-nitrophenyl)-3-phenethyl-5H-thiazolo [3, 2-a] pyrimidine-6-carboxylate (**7a**). Color less solid, R_f 0.40; (dichloromethane: ethyl acetate, 1:1 v/v). Yield: 81%; m.p.: 236-238 ºC; IR: 3055, 2981, 2894, 2684, 2360, 1683, 1591, 1527, 1348, 1110, 1010, 748 cm^{-1}; ^{1}H NMR (DMSO-d$_6$) δ 1.22 (*t*, 3H), 2.40 (*s*, 3H), 2.63-2.71 (m, 2H), 2.78-2.84 (m, 1H), 3.07-3.13 (m, 1H), 4.01-4.19 (m, 2H), 6.64 (s, 1H), 7.09-7.25 (m, 6H), 7.71 (t, 1H), 7.78-7.80 (m, 1H), 8.21-8.25 (m, 2H); ^{13}C NMR (DMSO-d$_6$) δ 13.9, 18.3, 27.2, 32.0, 57.5, 60.6, 101.5, 108.7, 122.1, 124.1, 126.3, 128.2, 128.3, 131.1, 133.6, 139.4, 140.6, 141.7, 147.8, 161.4, 163.7. HRMS cald for $C_{24}H_{24}N_3O_4S$ (M+H) 450.1488; found 450.1475 (TOF MS ES$^+$).

The same experimental method was adopted for the preparation of the remaining title compounds (**7b-j**).

Powder Pattern and single crystal structure comparison for compound 6a

Room temperature x-ray powder patterns were obtained using monochromated CuKα radiation (λ= 1.54178 Å) on a Bruker Proteum Diffraction System equipped with Helios multilayer optics, an APEX II CCD detector and a Bruker MicroStar microfocus rotating anode x-ray source

operating at 45kV and 60mA. The powders were mixed with a small amount of Paratone N oil to form a paste that was then placed in a small (< 0.5 mm.) nylon kryoloop and mounted on a goniometer head. The specimen was then positioned at the goniometer center-of-motion by translating it on the goniometer head. Three overlapping 1 minute 180º φ-scans were collected using the Bruker Apex2 V2010.3-0 software package[53] with the detector at 2θ = 30º, 60º and 90º using a sample-to-detector distance of 50.0 mm. These overlapping scans were merged and converted to a RAW file using the Pilot/XRD2 evaluation option that is part of the APEX2 software package. This RAW file was then processed using the Bruker EVA powder diffraction software package.

Crystal data and structure determination of the synthesized compound

Colorless single-domain crystals of 2*H*-thiazolo [3,2-a]pyrimidines (**6a**) and (**6e**) and 5*H*-thiazolo[3,2-a]pyrimidines (**7a**) and (**7i**) suitable for single-crystal x-ray diffraction studies were grown from methanol. Crystallographic data and refinement results are summarized in Table 1 for **6a** and **6e** and in Table 2 for **7a** and **7i**. Full hemispheres of redundant diffracted intensities [5237 (**6a**), 5233 (**6e**), 5237 (**7a**) or 4438 (**7i**) 2-5 second frames for each with an ω- or ϕ-scan width of 0.50°] were measured at 100(2)K for single-domain specimens of all four compounds using monochromated CuKα radiation (λ= 1.54178 Å) on a dual-detector Bruker Proteum Single Crystal Diffraction System equipped with Helios high-brilliance multilayer optics, an APEX II CCD (**6a**, **6e** and **7a**) or Platinum 135 (**7i**) CCD detector and a Bruker MicroStar microfocus rotating anode x-ray source operating at 45kV and 60mA. Sample-to-detector distances of 50 mm (**6a**, **6e** and **7a**) and 180 mm (**7i**) were used to collect data. Lattice constants were determined with the Bruker SAINT software package using peak centers for 9875 (**6a**), 9869 (**6e**), 8270 (**7a**) and 9796 (**7i**) reflections. Integrated reflection intensities were produced for all structures using the Bruker program SAINT[54] and the data were corrected empirically for variable absorption effects using equivalent reflections. The Bruker software package SHELXTL was used to solve the structure using "direct methods" techniques. All stages of weighted full-matrix least-squares refinement were conducted using F_o^2 data with the SHELXTL v2010.3-0 software package.[55]

The final structural models for all four structures incorporated anisotropic thermal parameters for all nonhydrogen atoms and isotropic thermal parameters for all hydrogen atoms. All hydrogen atoms were located in a difference Fourier and then included in the structural model as individual isotropic atoms whose parameters were allowed to vary in least-squares refinement cycles. The methyl groups for **7i** were incorporated into the final structural model as rigid groups (using idealized sp^3-hybridized geometry and a C-H bond length of 0.98 Å) that were allowed to rotate freely about their C-C bonds in least-squares refinement cycles; the isotropic thermal parameters for the methyl hydrogen atoms were allowed to vary. The structures of **6a, 6e, 7a,** and **7i** are shown in Figures 1-2 and 4-6, respectively. Tables of fractional atomic coordinates, thermal parameters, bond lengths and angles, torsion angles and hydrogen bonding parameters for the structures of **6a, 6e, 7a,** and **7i** are given in the supplementary material.

3. RESULTS AND DISCUSSION

AChE inhibitors design

In order to develop drugs for Alzheimer's treatment[56, 57], a series of compounds were designed and their capacity to inhibit AChE activity was predicted by QSAR and molecular docking studies. Pharmacokinetic properties like absorption, distribution, metabolism, and excretion (ADME) were also defined to predict their adverse effects in the system. The QSAR analysis helped to derive highly applicable models that permitted the design of novel and reactive molecules.[57] Preliminary structure–activity relationship (SAR) studies indicated that the pyrimidine moiety is required for inhibition of AChE activity.[38, 58] This is consistent with pyrimidine derivatives being widely used as treatment of AD at different stages.[38-41] Pyrimidine derivatives have been useful for treating diseases associated with the deposition of beta-amyloid peptide in the brain (such as Alzheimer's disease [39]), and as microtubule affinity regulating kinase inhibitors or in the treatment or prevention of tauopathies.

As acetylcholinesterase (AChE) plays a key role in the regulation of the cholinergic system, inhibition of AChE has emerged as one of the most promising strategies for the treatment of AD.

[38, 59-61] Pyrimidine derivatives were therefore built and screened virtually using the docking method.

The goal of the present work was to synthesize AChE inhibitor drugs with enhanced bioavailability by increasing the number of aromatic substituents on the basic pyrimidine core. This should increase affinity for the dual binding sites of AChE and increase the acetylcholine level in the brain. The *5H*-thiazolo [3,2-a]pyrimidines provide the minimum functionality necessary to achieve good binding deep in the AChE dual active site. Since pyrimidine species also provide remarkable enhancements of permeation across biological membranes and of oral bioavailability, we set out to design and synthesize small drug molecules incorporating substituted *2H*-thiazolo [3,2-a]pyrimidine and *5H*-thiazolo [3,2-a]pyrimidine moieties (Schemes 2) that might have the capacity to cross the BBB and inhibit AChE activity. To further enhance the potential for inhibition, *5H*-thiazolo[3,2-a]pyrimidines were designed to incorporate significant intramolecular flexibility by linking polar groups having highly favorable enthalpic interactions with conserved enzyme residues in the dual binding site.

Chemistry

A series of novel *2H*-thiazolo [3,2-a]pyrimidine and *5H*-thiazolo[3,2-a]pyrimidine derivatives were synthesized with variations at the aromatic rings and their linking group. As shown in Scheme 2, various aromatic aldehydes, thiourea and ethylacetoacetate/methylacetoacetate (**2**) were mixed with polyphosphoric acid (PPA) (5 mol %) in ethanol (10mL) in a one-pot, three-component reaction. The reaction mixture was refluxed with stirring for 6-8 hours. PPA is an extremely efficient catalyst for this reaction. All the reactions were carried out following this general procedure. On each occasion, the spectral data (IR, NMR, and HRMS) of prepared known compounds were identical with those reported in the literature. Further, the intermediate dihydropyrimidines **4a-4j** were reacted with 1-bromo-4-phenylbutan-2-one at room temperature for 6-12 h to give a solid. This was filtered and washed with water to obtain compounds **6a-6j** in high yields (80–95%). Since this resulted in diastereomers having two chiral centers i.e **6a-6j,** we employed simple diastereomeric crystallization to separate them. Diastereomeric crystallization is used so widely that it provides a measure for judging alternative processes.[62] The salts formed are diastereomers with different physical properties and may be separated in a number of ways, for example by chromatography, but the most efficient method of separating such diastereomers

is by crystallization. Many significant pharmaceuticals are resolved using diastereomeric crystallization.[62] This is a widely used technique in manufacturing processes for providing single-isomer drugs produced by synthetic means. A study of a representative group of market drugs shows that more than 65% are manufactured by methods involving diastereomeric crystallization of salts.[63, 64]

We have preferentially isolated a single compound (diasteromer B) from the equilibrium shown in Scheme 2 using diastereomeric crystallization of the HBr salt (the HBr was produced from the reaction of **4a**-**4j** with **5a**-**5j**). Salts **6a** and **6e** were the principal crystalline material that formed in methanol. This was verified by determining the solid-state structures for single crystals of **6a** and **6e** using x-ray diffraction (Table 1) and obtaining an experimental PXRD pattern for the bulk solid. This experimental powder pattern for the bulk was then compared with a calculated powder using atomic coordinates for the (single) crystal structures for **6a** and **6e** (Figure 1 & 2).

Insert Scheme1, Figure 1-2 & Table 1

Figures 3 & 4 each show a black experimental powder pattern for the dry bulk material from the crystallization vial that is superimposed with a red powder pattern calculated for the single crystal structures of compounds **6a** and **6e**, respectively**.** Each black pattern was obtained with some of the dry bulk solid from the crystallization vial that had been ground to a powder. Each red pattern was calculated with atomic coordinates resulting from the single crystal structure determination of compound **6a** or **6e** using the public-domain Mercury software package[65]. Clearly, the peaks for both sets of superimposed patterns occur at the same places and generally have the same relative heights. This indicates the significant presence of just one crystalline material (**6a** & **6e**) in the bulk solid that resulted when all of the solvent evaporated. Both bulk samples also contain a minor component that is an amorphous solid.

Insert Figure 3 & 4

Compounds **6a-6j** were further refluxed for 6-8 h to form the compounds **7a-7j** in high yields. The synthetic route utilized to make our target "AChE inhibitors" compounds **6a-6j** and **7a-7j** is shown in **Scheme 1**. The chemical structures of the new compounds were confirmed by elemental analysis, IR, ^{1}H NMR, ^{13}C NMR spectral- and HRMS; the data are presented in the

experimental section. Structures for compounds **6a**, **6e**, **7a** (Figure 5 & Table 2) and **7i** (Figure 6 & Table 2) were further confirmed by single crystal XRD.

Insert Figure 5 -6 & Table 2

Insert Scheme 2 & Table 3

QSAR study

Three-dimensional structures were built for compounds **6a**-**6j** and **7a**-**7j** and optimized in a MOE working environment. Molecular dynamics simulations were carried out for each molecule and molecular descriptors were determined followed by QSAR linear regression study (Table 4). The correlation model showed a linear plot for both measured IC_{50} values and values predicted for the training set of molecules (Figure 7).[23, 38, 58, 61] The correlation analysis showed an RMSD of 4.0 and $\mathbf{r^2}$ value of 0.86. This linearity for the model indicates the reliability of QSAR to compare and predict the activity of a test set molecules (Figure 8).

QSAR Descriptors

Insert Table 4 & Figure 7 -8

Principal Component Analysis

A principal component analysis using the QSAR descriptors showed that the first two PCA eigenvectors included 100% of the variance. All the data values were found to lie in the range of -3 > PCA 1 < +3 and -2 > PCA 2 < +2, where each spot in the plot represents a molecule. Most interestingly, the most active compounds in our data set, as shown in magenta, are distinctly isolated from the other molecules within the region: 0 > PCA1< 3.0 and 0.5 > PCA2 < - 3.0 (Figure 9). This could provide an addition criterion for compound selection.

Insert Figure 9

Molecular docking of AChE inhibitors:

Molecular modeling has often been proven to be a powerful tool for rationalizing ligand-target interactions and for making this information available to virtual screening techniques. Molecular modeling studies were performed using human AChE, since they represent the pharmacological target for the development of new drugs for the treatment of AD. The crystal structure of AChE protein (1B41) was loaded into MOE (Molecular Operating Environment (MOE, version 2012.10)[27] with a resolution of 2.76 Å and a library was constructed for all the lead molecules[66]. The binding site of human AChE protein was identified from PDBSum[67] and the residues D74, W86, N87, G120, G121, G122, Y124, S125, G126, L130, E202, S203, F297, Y337, F338, Y341, H447, G448, and I451, were found to be interacting residues as shown in Figures 10-15.

Docking of Donepezil with AChE (1B41)

As a validation of the docking procedure (Figure 10), the structure of the 1B41-Donepezil complex was analyzed and the binding affinity (GBV/WSA scoring function) and Generalized Born solvation energy were calculated.

Insert Figure 10

The binding affinity (GBV!/WSA scoring function) of Donepezil was calculated as -8.0 (+/- 0.3) kcal/mole, and Generalized Born solvation energy as -28.2(+/- 1.0) kcal/mole. Donepezil therefore binds with >3 kcal/mole greater solvation energy than our predicted lead compounds, **6c**, **7c** and **7h** (Table 5). Donepezil also has a 0.3 - 0.6 kcal/mole lower calculated affinity than compounds **6c**, **7c** and **7h** but this is within the 2σ limit. However Donepizel has slightly higher solvation energy than the other compounds. It's tempting to suggest it gains additional binding affinity by its desolvation stabilization within the aromatic lined "groove" site (PAS region) of the human AChE receptor, as compared to our inhibitor candidates.

Therefore, the docking procedure that was used gives us information about important ligand-receptor interactions and ligand affinities, using a protocol including molecular mechanics, genetic algorithm, and Lamarckian GA calculations. On the basis of the obtained hits, 5*H*-thiazolo [3,2-a]pyrimidine and 2*H*-thiazolo [3,2-a]pyrimidine derivatives emerged as promising candidates. Selected conformers of compounds were docked into the human AChE structure (PDB code 1B41), shown in Figures 11-15.

Insert Figure 11-14

Among all docking conformations, compounds **7c** had the best least docking score of -8.6 kcal/mole and the next best docking scores were for compounds **6c** and **7h** with docking scores **-**8.3, and **-**8.3**,** respectively. **7c** was found to form an arene-hydrogen bond with Gly121. These three ligands had the first best least docking scores with stable ligand pose interactions in the docking sphere followed by the remaining lead compounds.

Insert Figure 15 & Table 5

Pharmacophore Model

AChE Inhibitor 4 Feature Pharmacophore Model

Insert Figure 16 & Table 6

The Pharmacophore model selected 13 out of 20 compounds in the database as hits. These are identified under "Comp ID". The column "$PRED_HITS" gives a calculated % Inhibition value from the QSAR model. The positive values are considered as active hits, which include compounds **6c, 6d, 6h, 7c** and **7h**.

ADME predictions[68, 69]

ADME properties are important conditions and major parts of pharmacokinetics. Viable drugs should have perfect ADME properties for it to be approved as a drug in clinical tests. The ADME predictions of the present 20 compounds show satisfactory results. Among the twenty, compounds **6a-6j** and **7a-7j** show good intestinal absorption. All of them show moderate permeability for *in vitro* Caco-2 cells and low permeability for *in vitro* MDCK cells. *In vivo* blood-brain barrier penetration capacity was predicted to have middle absorption to the CNS (Central Nervous System) for the compounds **6c, 6g, 6h,** and **7a-7j** whereas low absorption to the CNS was observed for the compounds **6a, 6b, 6d, 6e, 6f, 6i,** and **6j**. Blood brain barrier penetration is a crucial pharmacokinetic property because CNS-active compounds must pass across it and CNS-inactive compounds must not pass across it to avoid CNS side effects. Generally, the degree to which any drug binds to plasma protein influences not only the drug

action but also its disposition and efficacy. Usually, the drug that is unbound to plasma proteins will be available for diffusion or transport across cell membranes and thereby finally interact with the target. Herein with respect to ADME, the percent of drug bound with plasma proteins was predicted and the compounds **6a-6j** and **7a-7j** were predicted to bind strongly. The predicted ADME properties and their values are shown in the table 7.

Insert Table 7

4. CONCLUSIONS AND FUTURE DIRECTIONS

This study described the design, synthesis, diastereomeric crystallization, docking, 2D QSAR and pharmacophore studies for a series of highly selective inhibitors of AChE. The pharmacophore model reflected the binding mode and important interactions of the ligands binding to the dual site of the enzyme. The ligand-oriented study used multiple contributions of ligand features to build a quantitative pharmacophore model from a training set of 20 AChE inhibitors with known IC_{50} values. The best pharmacophore model contained four basic pharmacophore features with a correlation coefficient of 0.90: two hydrogen bond acceptors and two hydrophobic interactions. This pharmacophore model was then applied to the novel set of 20 test molecules that have been synthesized and described in the chemistry section. Taken individually, the docking, 2D QSAR and pharmacophore studies for the test set each indicated that at least six of the twenty test compounds should be reasonable inhibitors of AChE. All test compounds showed proper drug-like 2D QSAR and ADMET properties. The ligand-protein complexes generated with molecular docking indicated that the six of the test molecules should be good AChE inhibitors since they showed good binding affinity with the dual sites of the enzyme receptor. Five of the twenty had good QSAR values and four of the twenty had good pharmacophore values. However, only three of the twenty test compounds (**6c**, **7c** and **7h**) had good docking, QSAR and pharmacophore values, Figure 17. It therefore seems that by combining all three of these evaluation procedures, large numbers of new compounds can be screened as possible inhibitors of AChE. Since the present results indicate that compounds **6c**, **7c** and **7h** should be excellent candidates for inhibition of AChE, we plan to use them as a

starting point for developing even more potent analogues for the treatment of the Alzheimer's disease.

Insert Figure 17

ACKNOWLEDGMENTS

This study was supported by grant awards (R01GM095355, R37AG037319, and PO1AG017490) from the National Institute of General Medical Sciences and the National Institute on Aging. The authors thank the National Science Foundation (grant CHE-0923449) and the University of Kansas for funds to purchase the x-ray instrumentation and computers.

ASSOCIATED CONTENT

Supporting Information: Experimental details and spectroscopic data of synthesized compounds ^{1}H, ^{13}C, NMR chromatograms and crystal structures supporting tables. This material is available free of charge via the Internet at http://pubs.acs.org.

ABBREVIATIONS

AChE, Acetylcholinesterase; ACh, acetylcholine; AD, Alzheimer's disease; AChEIs, Acetylcholinesterase inhibitors; Aβ, amyloid beta; QSAR, quantitative structure–activity relationship; CoMFA, comparative molecular field analysis; ADMET, absorption, distribution, metabolism and excretion and toxicity; FDA, Food and Drug Administration; BBB, blood brain barrier; Caco2, human colon adenocarcinoma; MDCK, Madin-Darby canine kidney; SAR, structure–activity relationship; CNS, central nervous system; MOE, molecular operating environment; RMSE, Root mean square error; PCA, Principle Component Analysis; PDB, Protein Data Bank; MMFF94x, The Merck Molecular Force Field;

References

1. Berman, H. M.; Bhat, T. N.; Bourne, P. E.; Feng, Z.; Gilliland, G.; Weissig, H.; Westbrook, J., The Protein Data Bank and the challenge of structural genomics. *Nat. Struct. Biol.* **2000,** *7* Suppl, 957-9.

2. Berman, H. M.; Westbrook, J.; Feng, Z.; Gilliland, G.; Bhat, T. N.; Weissig, H.; Shindyalov, I. N.; Bourne, P. E., The Protein Data Bank. *Nucleic. Acids. Res.* **2000,** *28,* 235-42.

3. Dastmalchi, S.; Hamzeh-Mivehroud, M.; Ghafourian, T.; Hamzeiy, H., Molecular modeling of histamine H3 receptor and QSAR studies on arylbenzofuran derived H3 antagonists. *J.Mol. Graph. & Mod.***2008,** *26,* 834-844.

4. Glaser, B., Psychiatry and paedophilia: a major public health issue. *Aust. N Z J Psychiatry.* **1998,** *32,* 162-7.

5. Hauptmann, S.; Scherping, I.; Drose, S.; Brandt, U.; Schulz, K. L.; Jendrach, M.; Leuner, K.; Eckert, A.; Muller, W. E., Mitochondrial dysfunction: an early event in Alzheimer pathology accumulates with age in AD transgenic mice. *Neurobiol. Aging.* **2009,** *30,* 1574-86.

6. Mao, Y.; Shang, Z.; Imai, Y.; Hoshino, T.; Tero, R.; Tanaka, M.; Yamamoto, N.; Yanagisawa, K.; Urisu, T., Surface-induced phase separation of a sphingomyelin/cholesterol/ganglioside GM1-planar bilayer on mica surfaces and microdomain molecular conformation that accelerates Abeta oligomerization. *Biochim. Biophys. Acta.* **2010,** *1798,* 1090-1099.

7. Park, S. K.; Pegan, S. D.; Mesecar, A. D.; Jungbauer, L. M.; LaDu, M. J.; Liebman, S. W., Development and validation of a yeast high-throughput screen for inhibitors of Abeta(4)(2) oligomerization. *Dis. Model. Mech.* **2011,** *4,* 822-831.

8. Stains, C. I.; Ghosh, I., When conjugated polymers meet amyloid fibrils. *ACS. Chem. Biol.* **2007,** *2,* 525-528.

9. Sun, F.; Knebelmann, B.; Pueyo, M. E.; Zouali, H.; Lesage, S.; Vaxillaire, M.; Passa, P.; Cohen, D.; Velho, G.; Antignac, C.; et al., Deletion of the donor splice site of intron 4 in the glucokinase gene causes maturity-onset diabetes of the young. *J. Clin. Invest.* **1993,** *92,* 1174-1180.

10. Alipour, M.; Khoobi, M.; Foroumadi, A.; Nadri, H.; Moradi, A.; Sakhteman, A.; Ghandi, M.; Shafiee, A., Novel coumarin derivatives bearing N-benzyl pyridinium moiety: Potent and dual binding site acetylcholinesterase inhibitors. *Bioorg. Med. Chem.* **2012,** *20*, 7214-7222.

11. Alipour, M.; Khoobi, M.; Foroumadi, A.; Nadri, H.; Moradi, A.; Sakhteman, A.; Ghandi, M.; Shafiee, A., Novel coumarin derivatives bearing N-benzyl pyridinium moiety: Potent and dual binding site acetylcholinesterase inhibitors. *Bioorg. Med. Chem.* **2012,** *20*, 7214-22.

12. Yankner, B. A.; Duffy, L. K.; Kirschner, D. A., Neurotrophic and Neurotoxic Effects of Amyloid Beta-Protein - Reversal by Tachykinin Neuropeptides. *Science.* **1990,** *250*, 279-282.

13. Iijima, K.; Liu, H. P.; Chiang, A. S.; Hearn, S. A.; Konsolaki, M.; Zhong, Y., Dissecting the pathological effects of human A beta 40 and A beta 42 in Drosophila: A potential model for Alzheimer's disease. *Proc. Natl. Acad. Sci. USA* **2004,** *101,* 6623-6628.

14. Tabet, N., Acetylcholinesterase inhibitors for Alzheimer's disease: anti-inflammatories in acetylcholine clothing! *Age. Ageing.* **2006,** *35,* 336-338.

15. Bolognesi, M. L.; Andrisano, V.; Bartolini, M.; Banzi, R.; Melchiorre, C., Propidium-based polyamine ligands as potent inhibitors of acetylcholinesterase and acetylcholinesterase-induced amyloid-beta aggregation. *J. Med. Chem.* **2005,** *48,* 24-27.

16. Savini, L.; Gaeta, A.; Fattorusso, C.; Catalanotti, B.; Campiani, G.; Chiasserini, L.; Pellerano, C.; Novellino, E.; McKissic, D.; Saxena, A., Specific targeting of acetylcholinesterase and butyrylcholinesterase recognition sites. Rational design of novel, selective, and highly potent cholinesterase inhibitors. *J. Med. Chem.* **2003,** *46,* 1-4.

17. Francis, P. T.; Palmer, A. M.; Snape, M.; Wilcock, G. K., The cholinergic hypothesis of Alzheimer's disease: a review of progress. *J.Neuro. Neurosur.& Psy.* **1999,** *66,* 137-147.

18. Allen, N. H. P.; Burns, A., The Treatment of Alzheimers-Disease. *J. Psychopharmacology.* **1995,** *9,* 43-56.

19. Ibach, B.; Haen, E., Acetylcholinesterase inhibition in Alzheimer's disease. *Cur.Pharma.Design.* **2004,** *10,* 231-251.

20. Birks, J., Cholinesterase inhibitors for Alzheimer's disease. *Cochrane. Database. of Systematic. Reviews.* **2006**, *1,* CD005593.

21. Wilcock, G.; Howe, I.; Coles, H.; Lilienfeld, S.; Truyen, L.; Zhu, Y.; Bullock, R.; Grp, G. G. S., A long-term comparison of galantamine and donepezil in the treatment of Alzheimer's disease. *Drugs & Aging.* **2003,** *20*, 777-789.

22. Bullock, R.; Touchon, J.; Bergman, H.; Gambina, G.; He, Y. S.; Rapatz, G.; Nagel, J.; Lane, R., Rivastigmine and donepezil treatment in moderate to moderately-severe Alzheimer's disease over a 2-year period. *Cur. Med. Res.& Opinion.* **2005,** *21*, 1317-1327.

23. Birks, J.; Harvey, R. J., Donepezil for dementia due to Alzheimer's disease (Review). *Cochrane. Database .of Systematic. Reviews.* **2006**, *25*, CD001190.

24. Loy, C.; Schneider, L., Galantamine for Alzheimer's disease and mild cognitive impairment. *Cochrane. Database. of Systematic. Reviews.* **2006**, *25*, CD001747.

25. Birks, J.; Evans, J. G.; Iakovidou, V.; Tsolaki, M.; Holt, F. E., Rivastigmine for Alzheimer's disease. *Cochrane. Database. of Systematic. Reviews.* **2000,** *4***, CD001191**.

26. Raves, M. L.; Harel, M.; Pang, Y. P.; Silman, I.; Kozikowski, A. P.; Sussman, J. L., Structure of acetylcholinesterase complexed with the nootropic alkaloid, (-)-huperzine A. *Nat. Struct. Biol.* **1997,** *4*, 57-63.

27. Chemical computing group releases MOE version 2002.03. *J. Chem.Education.* **2002,** *79*, 951-951.

28. Abad, N. H.; Doulatabad, N. S.; Mohammadi, A.; Srazi, H. R., Treatment of Visual Hallucinations in Schizophrenia by Acetylcholinesterase Inhibitors: a case report. *Iran. J. Psychiatry.* **2011,** *6*, 161-163.

29. Park, S. K.; Pegan, S. D.; Mesecar, A. D.; Jungbauer, L. M.; Ladu, M. J.; Liebman, S. W., Development and validation of a yeast high-throughput screen for inhibitors of A beta(42) oligomerization. *Dis. Model. Mech.* **2011,** *4*, 822-831.

30. Stains, C. I.; Ghosh, I., When conjugated polymers meet amyloid fibrils. *ACS. Chem. Biol.* **2007,** *2*, 525-528.

31. Mori, F.; Lai, C. C.; Fusi, F.; Giacobini, E., Cholinesterase-Inhibitors Increase Secretion of Apps in Rat-Brain Cortex. *Neuroreport* **1995,** *6*, 633-636.

32. Giacobini, E., Cholinesterases: New roles in brain function and in Alzheimer's disease. *Neurochemical. Research.* **2003,** *28*, 515-522.

33. Francis, P. T.; Nordberg, A.; Arnold, S. E., A preclinical view of cholinesterase inhibitors in neuroprotection: do they provide more than symptomatic benefits in Alzheimer's disease? *Trends in Pharmacological. Sciences.* **2005,** *26*, 104-111.

34. Hardy, J.; Selkoe, D. J., Medicine - The amyloid hypothesis of Alzheimer's disease: Progress and problems on the road to therapeutics. *Science* **2002,** *297*, 353-356.

35. Selkoe, D. J., Normal and Abnormal Biology of the Beta-Amyloid Precursor Protein. *Annual. Review.of Neuroscience.* **1994,** *17*, 489-517.

36. Inestrosa, N. C.; Alvarez, A.; Perez, C. A.; Moreno, R. D.; Vicente, M.; Linker, C.; Casanueva, O. I.; Soto, C.; Garrido, J., Acetylcholinesterase accelerates assembly of amyloid-beta-peptides into Alzheimer's fibrils: Possible role of the peripheral site of the enzyme. *Neuron* **1996,** *16*, 881-891.

37. Castro, A.; Martinez, A., Peripheral and Dual Binding Site Acetylcholinesterase Inhibitors: Implications in treatment of Alzheimer's Disease. *Mini-Rev. in Med.Chem.***2001,** *1*, 267-272.

38. Zhi, H.; Chen, L. M.; Zhang, L. L.; Liu, S. J.; Wan, D. C. C.; Lin, H. Q.; Hu, C., Design, synthesis, and biological evaluation of 5H-thiazolo[3,2-a]pyrimidine derivatives as a new type of acetylcholinesterase inhibitors. *Arkivoc.* **2008**, 266-277.

39. Rivkin, A.; Ahearn, S. P.; Chichetti, S. M.; Kim, Y. R.; Li, C. M.; Rosenau, A.; Kattar, S. D.; Jung, J.; Shah, S.; Hughes, B. L.; Crispino, J. L.; Middleton, R. E.; Szewczak, A. A.; Munoz, B.; Shearman, M. S., Piperazinyl pyrimidine derivatives as potent gamma-secretase modulators. *Bioorg. Med. Chem. Lett.* **2010,** *20*, 1269-1271.

40. Messer, W. S., Jr.; Rajeswaran, W. G.; Cao, Y.; Zhang, H. J.; el-Assadi, A. A.; Dockery, C.; Liske, J.; O'Brien, J.; Williams, F. E.; Huang, X. P.; Wroblewski, M. E.; Nagy, P. I.; Peseckis, S. M., Design and development of selective muscarinic agonists for the treatment of Alzheimer's disease: characterization of tetrahydropyrimidine derivatives and development of new approaches for improved affinity and selectivity for M1 receptors. *Pharm. Acta. Helv.* **2000,** *74*, 135-40.

41. Kypta, R. M., GSK-3 inhibitors and their potential in the treatment of Alzheimer's disease. *Exp.Opin. Ther.Patents.* **2005,** *15*, 1315-1331.

42. Rivkin, A.; Ahearn, S. P.; Chichetti, S. M.; Kim, Y. R.; Li, C. M.; Rosenau, A.; Kattar, S. D.; Jung, J.; Shah, S.; Hughes, B. L.; Crispino, J. L.; Middleton, R. E.; Szewczak, A. A.; Munoz, B.; Shearman, M. S., Piperazinyl pyrimidine derivatives as potent gamma-secretase modulators. *Bioorg. Med. Chem. Lett.* **2010,** *20*, 1269-1271.

43. Timm, T.; von Kries, J. P.; Li, X. Y.; Zennpel, H.; Mandelkow, E.; Mandelkow, E. M., Microtubule Affinity Regulating Kinase Activity in Living Neurons Was Examined by a Genetically Encoded Fluorescence Resonance Energy Transfer/Fluorescence Lifetime Imaging-

based Biosensor INHIBITORS WITH THERAPEUTIC POTENTIAL. *J. Biol. Chem.* **2011,** *286*, 41711-41722.

44. Ono, M.; Hayashi, S.; Matsumura, K.; Kimura, H.; Okamoto, Y.; Ihara, M.; Takahashi, R.; Mori, H.; Saji, H., Rhodanine and Thiohydantoin Derivatives for Detecting Tau Pathology in Alzheimer's Brains. *Acs. Chem. Neuroscienc.e* **2011,** *2*, 269-275.

45. Heritage, T. W.; Ferguson, A. M.; Turner, D. B.; Willett, P., EVA: A novel theoretical descriptor for QSAR studies. *Persp. . Drug. Discovery. & Design.* **1998,** *9-11*, 381-398.

46. Todeschini, R.; Gramatica, P., New 3D molecular descriptors: The WHIM theory and QSAR applications. *Perspectives in Drug Discovery and Design* **1998,** *9-11*, 355-380.

47. Vilar, S.; Cozza, G.; Moro, S., Medicinal Chemistry and the Molecular Operating Environment (MOE): Application of QSAR and Molecular Docking to Drug Discovery. *Cur. Top. Med. Chem.* **2008,** *8*, 1555-1572.

48. Irvine, J. D.; Takahashi, L.; Lockhart, K.; Cheong, J.; Tolan, J. W.; Selick, H. E.; Grove, J. R., MDCK (Madin-Darby canine kidney) cells: A tool for membrane permeability screening. *J Pharm. Sci.* **1999,** *88*, 28-33.

49. Zhao, Y. H.; Le, J.; Abraham, M. H.; Hersey, A.; Eddershaw, P. J.; Luscombe, C. N.; Butina, D.; Beck, G.; Sherborne, B.; Cooper, I.; Platts, J. A., Evaluation of human intestinal absorption data and subsequent derivation of a quantitative structure-activity relationship (QSAR) with the Abraham descriptors. *J.Pharm. Sci.* **2001,** *90*, 749-84.

50. Vilar, S.; Cozza, G.; Moro, S., Medicinal chemistry and the molecular operating environment (MOE): application of QSAR and molecular docking to drug discovery. *Cur.Top. Med. Chem.* **2008,** *8*, 1555-72.

51. Vilar, S.; Gonzalez-Diaz, H.; Santana, L.; Uriarte, E., QSAR model for alignment-free prediction of human breast cancer biomarkers based on electrostatic potentials of protein pseudofolding HP-lattice networks. *J. Comput. Chem.***2008,** *29*, 2613-22.

52. Yao, J.; Irwin, R. W.; Zhao, L.; Nilsen, J.; Hamilton, R. T.; Brinton, R. D., Mitochondrial bioenergetic deficit precedes Alzheimer's pathology in female mouse model of Alzheimer's disease. *Proc. Natl. Acad. Sci. U S A* **2009,** *106*, 14670-5.

53. Data Collection: SMART Software in APEX2 v2010.3-0 Suite. Bruker-AXS, 5465 E. Cheryl Parkway, Madison, WI 53711-5373 USA. .

54. Data Reduction: SAINT Software in APEX2 v2010.3-0 Suite. Bruker-AXS, 5465 E. Cheryl Parkway, Madison, WI 53711-5373 USA. .

55. Refinement: SHELXTL v2010.3-0. Bruker-AXS, 5465 E. Cheryl Parkway, Madison, WI 53711-5373 USA.

56. Xie, Y.; Deng, S.; Chen, Z.; Yan, S.; Landry, D. W., Identification of small-molecule inhibitors of the Abeta-ABAD interaction. *Bioorg. Med. Chem. Lett.* **2006,** *16*, 4657-60.

57. Valasani, K. R.; Hu, G.; Chaney, M. O.; Yan, S. S., Structure-Based Design and Synthesis of Benzothiazole Phosphonate Analogues with Inhibitors of Human ABAD-Abeta for Treatment of Alzheimer's Disease. *Chem. Biol. Drug. Des.* **2012,** *81*, 238-349.

58. Zhi, H.; Chen, L. M.; Zhang, L. L.; Liu, S. J.; Wan, D. C. C.; Lin, H. Q.; Hu, C., Design, Synthesis, and Biological Evaluation of 5H-Thiazolo[3,2-a]pyrimidine-6-carboxylic Acid Ethyl Ester Derivatives as a Novel Series of Acetylcholinesterase Inhibitors. *Chemical. Research. in Chinese Universities.* **2009,** *25*, 332-337.

59. Dorronsoro, I.; Castro, A.; Martinez, A., Peripheral and dual binding site inhibitors of acetylcholinesterase as neurodegenerative disease-modifying agents. *Exp. Opin. Ther. Patents.* **2003,** *13*, 1725-1732.

60. Ma, H. J.; Xie, R. L.; Zhao, Q. F.; Mei, X. D.; Ning, J., Synthesis and Insecticidal Activity of Novel Carbamate Derivatives as Potential Dual-Binding Site Acetylcholinesterase Inhibitors. *J. Agri. & Food. Chem.***2010,** *58*, 12817-12821.

61. Leonetti, F.; Cappa, A.; Maccallini, C.; Carotti, A., Synthesis of potential dual binding site acetylcholinesterase inhibitors through an efficient solid phase approach based on the Mitsunobu reaction. *Arkivoc.* **2004**, 272-285.

62. Ruano, J. L. G.; Rodriguez, J.; Alcudia, F.; Llera, J. M.; Olefirowicz, E. M.; Eliel, E. L., Conformational-Analysis .47. The Stereochemistry of Sulfur Organic-Compounds .21. The Conformation of Oxanes with Sulfur Substituents. *J. Org. Chem.***1987,** *52*, 4099-4107.

63. Ahuja, S., ANYL 406-Are chiral separations of drugs really easy? *Abstracts of Papers of the American Chemical Society.* **2007,** 234.

64. Ahuja, S., Chiral Separations - an Overview. *Acs. Symposium. Series.* **1991,** *471*, 1-26.

65. Macrae, C. F.; Bruno, I. J.; Chisholm, J. A.; Edgington, P. R.; McCabe, P.; Pidcock, E.; Rodriguez-Monge, L.; Taylor, R.; van de Streek, J.; Wood, P. A., Mercury CSD 2.0 - new

features for the visualization and investigation of crystal structures. *J. Appl. Crystall.* **2008,** *41*, 466-470.

66. Davies, R. J.; Pierce, A. C.; Forster, C.; Grey, R.; Xu, J.; Arnost, M.; Choquette, D.; Galullo, V.; Tian, S. K.; Henkel, G.; Chen, G.; Heidary, D. K.; Ma, J.; Stuver-Moody, C.; Namchuk, M., Design, synthesis, and evaluation of a novel dual FMS-like tyrosine kinase 3/stem cell factor receptor (FLT3/c-KIT) inhibitor for the treatment of acute myelogenous leukemia. *J.Med. Chem.* **2011,** *54*, 7184-92.

67. Laskowski, R. A., PDBsum: summaries and analyses of PDB structures. *Nucleic Acids Res.* **2001,** *29*, 221-2.

68. Crivori, P.; Cruciani, G.; Carrupt, P. A.; Testa, B., Predicting blood-brain barrier permeation from three-dimensional molecular structure. *J.Med. Chem.* **2000,** *43*, 2204-2216.

69. Nielsen, P. A.; Andersson, O.; Hansen, S. H.; Simonsen, K. B.; Andersson, G., Models for predicting blood-brain barrier permeation. *Drug Discovery Today.* **2011,** *16*, 472-475.

70. Liu, Q. J.; Pan, N.; Xu, J. H.; Zhang, W. W.; Kong, F. P., Microwave-Assisted and Iodine-Catalyzed Synthesis of Dihydropyrimidin-2-Thiones Via Biginelli Reaction under Solvent-Free Conditions. *Synthetic Communications* **2013,** *43*, 139-146.

71. Lu, J.; Ma, H. R., Iron(III)-catalyzed synthesis of dihydropyrimidinones. Improved conditions for the Biginelli reaction. *Synlett* **2000**, *1*, 63-64.

72. Wang, Z. T.; Xu, L. W.; Xia, C. G.; Wang, H. Q., Novel Biginelli-like three-component cyclocondensation reaction: efficient synthesis of 5-unsubstituted 3,4-dihydropyrimidin-2(1H)-ones. *Tetrahedron Letters* **2004,** *45*, 7951-7953.

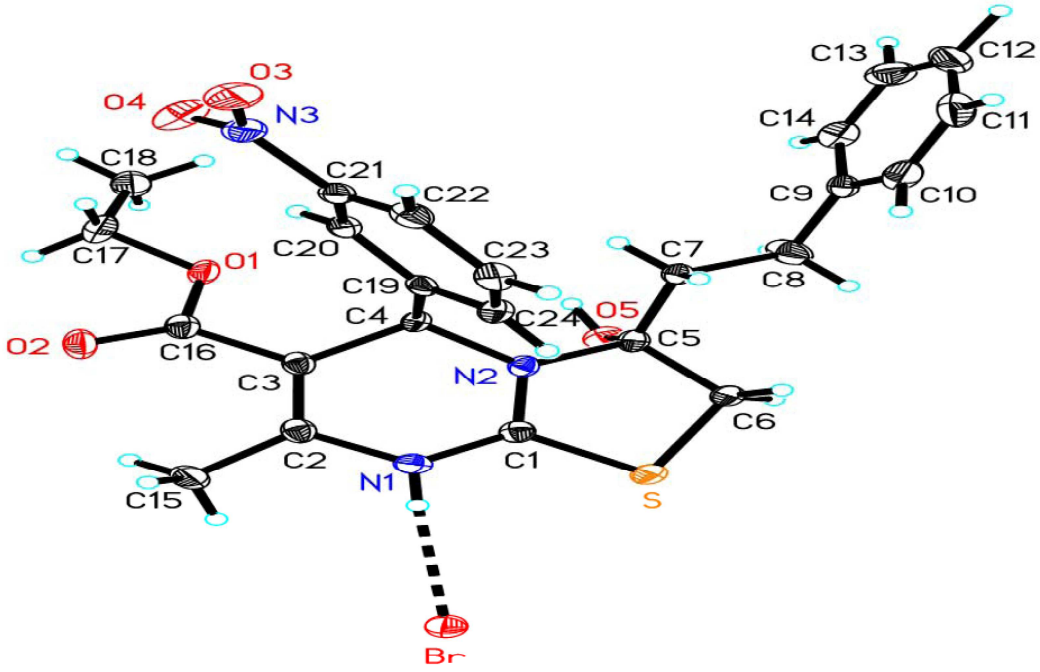

Figure 1. Crystal structure for HBr salt of **6a** showing 50% probability displacement ellipsoids and atom-numbering scheme

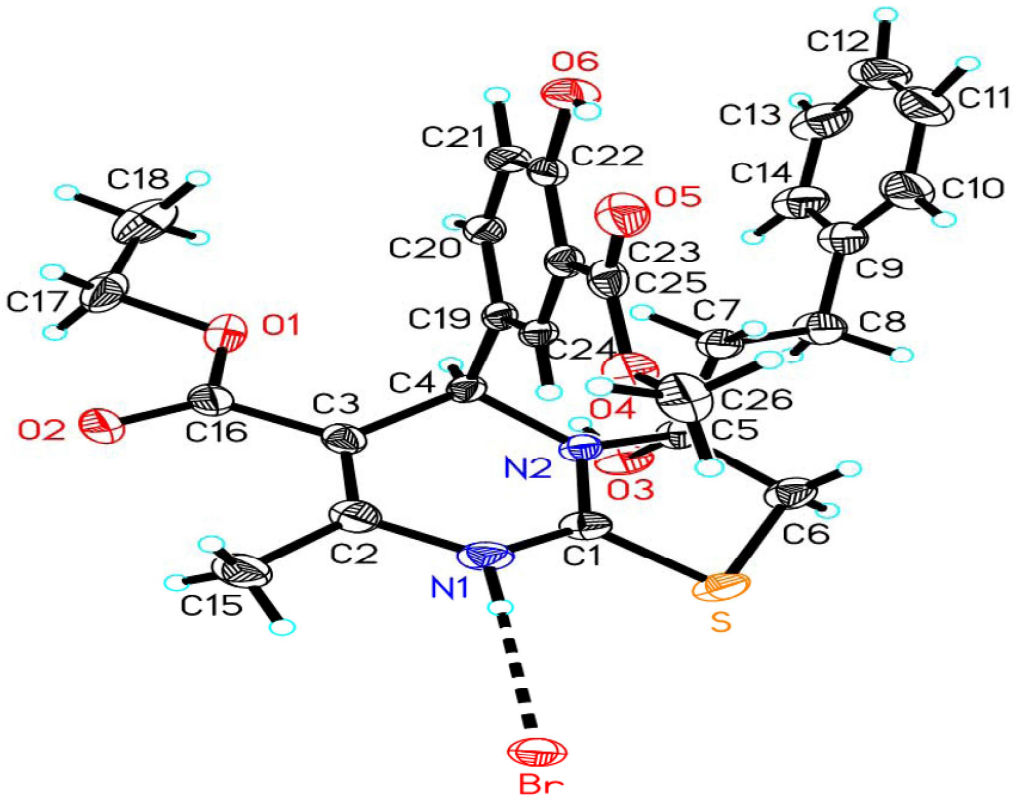

Figure 2. Crystal structure for HBr salt of **6e** showing 50% probability displacement ellipsoids and atom-numbering scheme

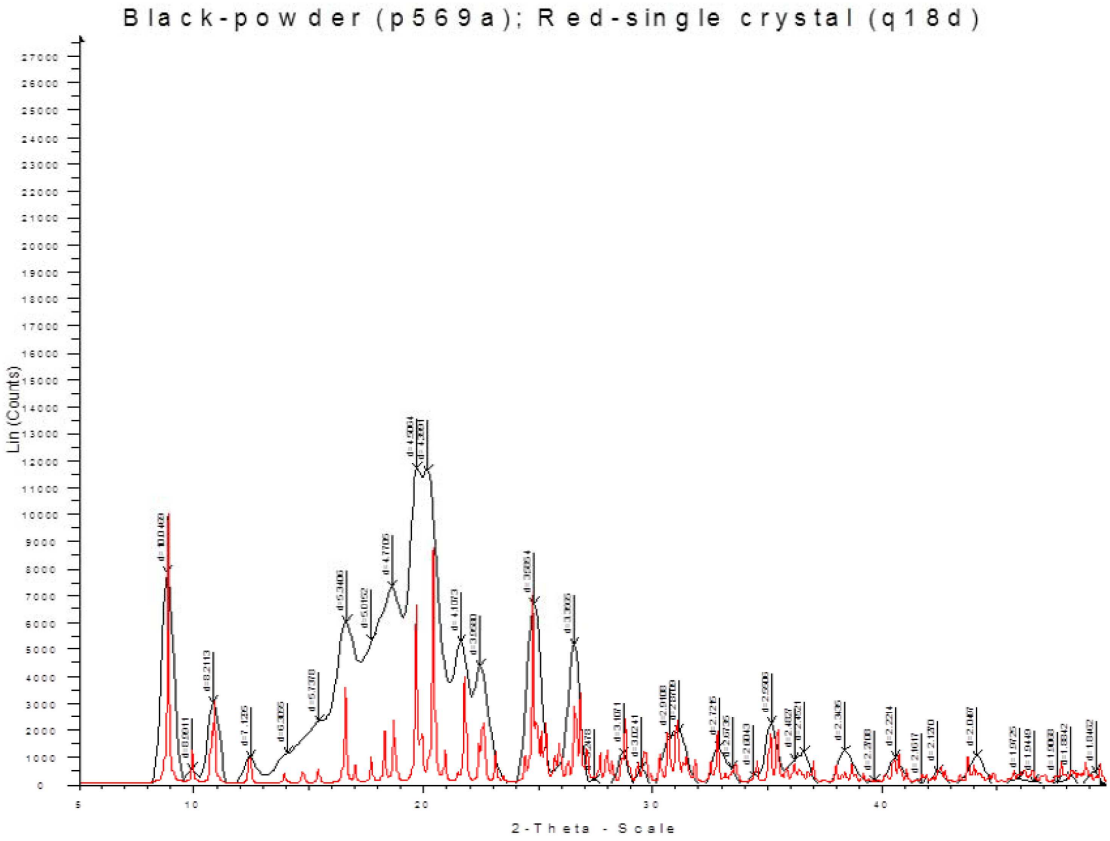

Figure 3. Superimposed experimental and calculated CuKα x-ray powder patterns for solids removed from evaporated solution for HBr salt of **6a**. Experimental PXRD of pulverized bulk solid (black) and PXRD calculated from single crystal structure determination (red) for HBr salt of **6a**.

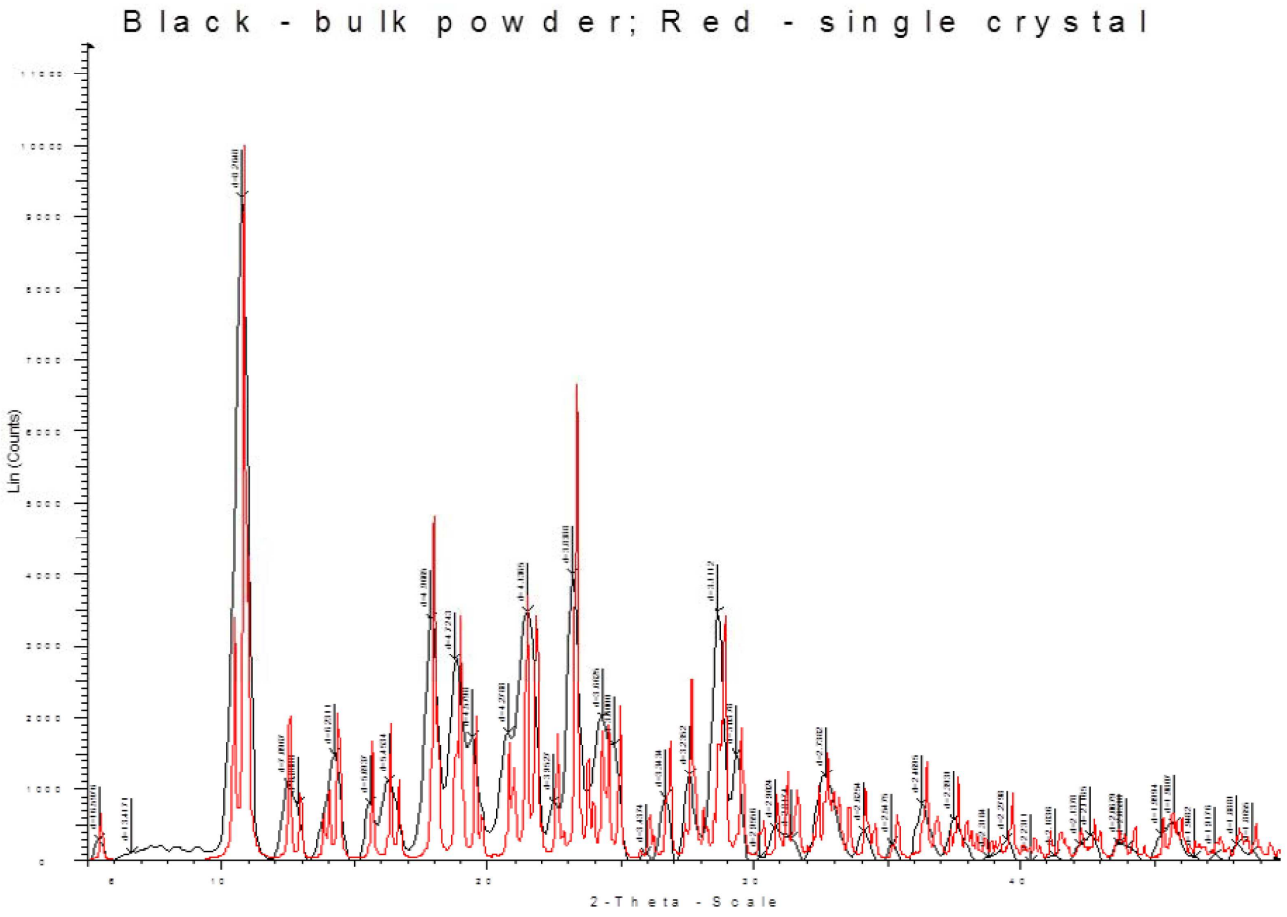

Figure 4. Superimposed experimental and calculated CuKα x-ray powder patterns for solids removed from evaporated solution for HBr salt of **6e**. Experimental PXRD of pulverized bulk solid (black) and PXRD calculated from single crystal structure determination (red) for HBr salt of **6e**.

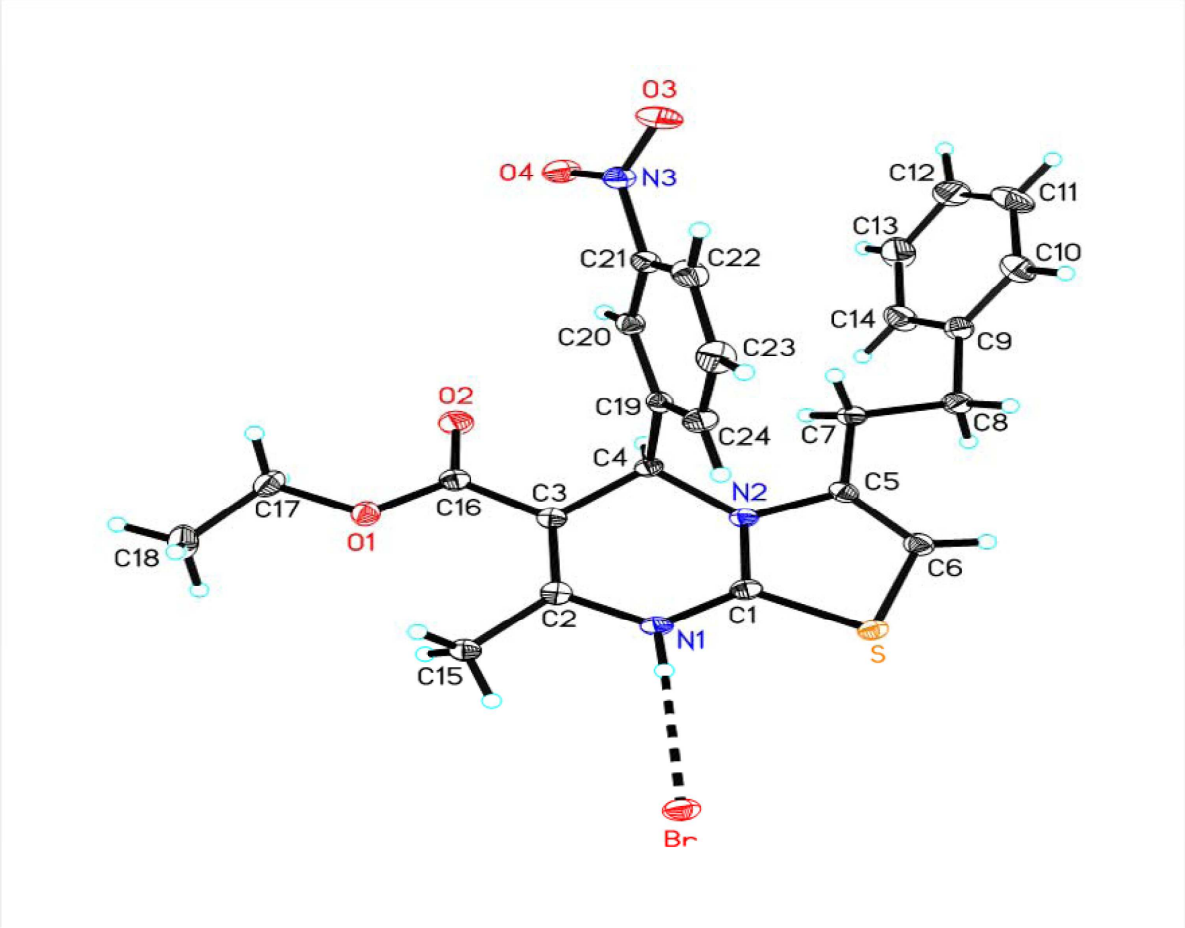

Figure 5. Crystal structure for HBr salt of **7a** showing 50% probability displacement ellipsoids and the atom-numbering scheme

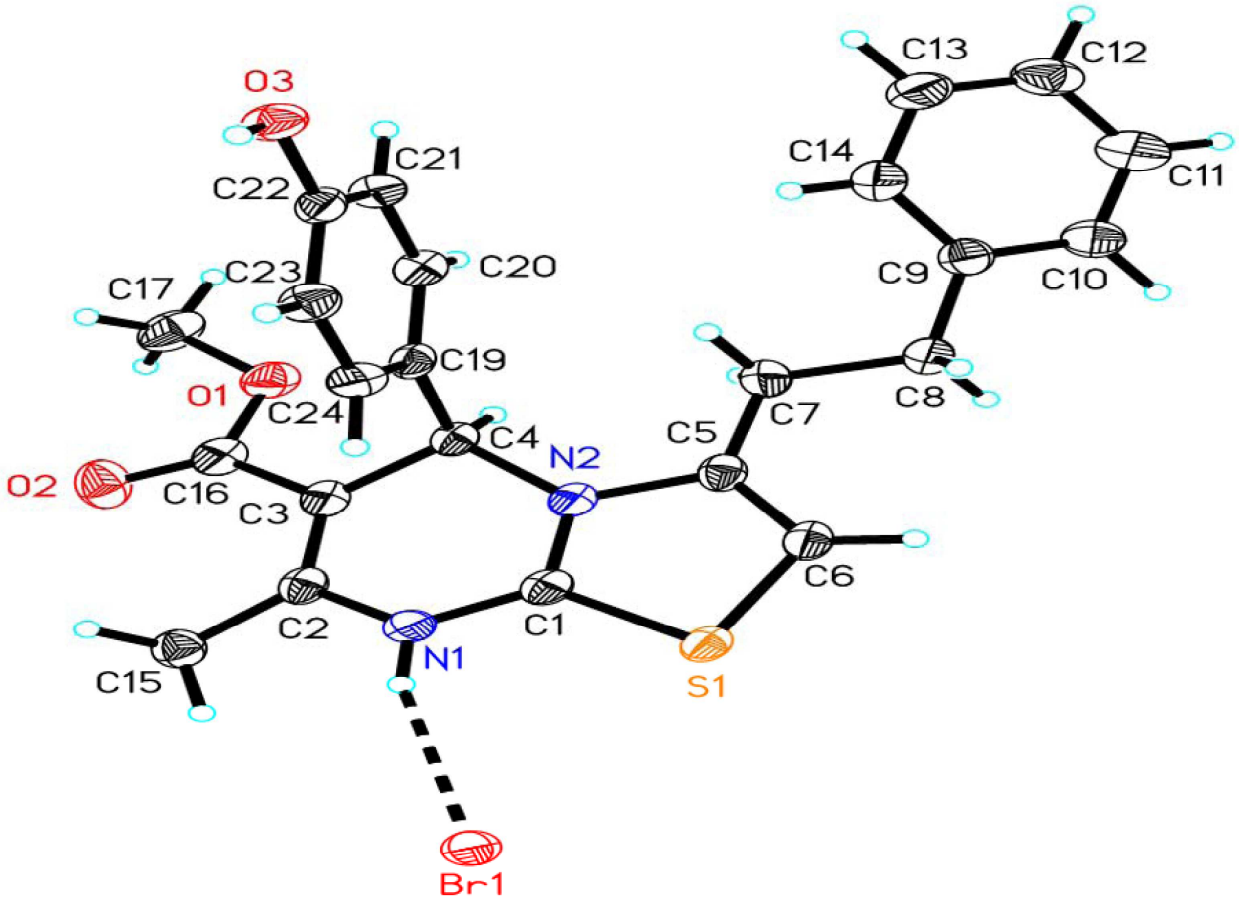

Figure 6. Crystal structure for HBr salt of **7i** showing 50% probability displacement ellipsoids and the atom-numbering scheme

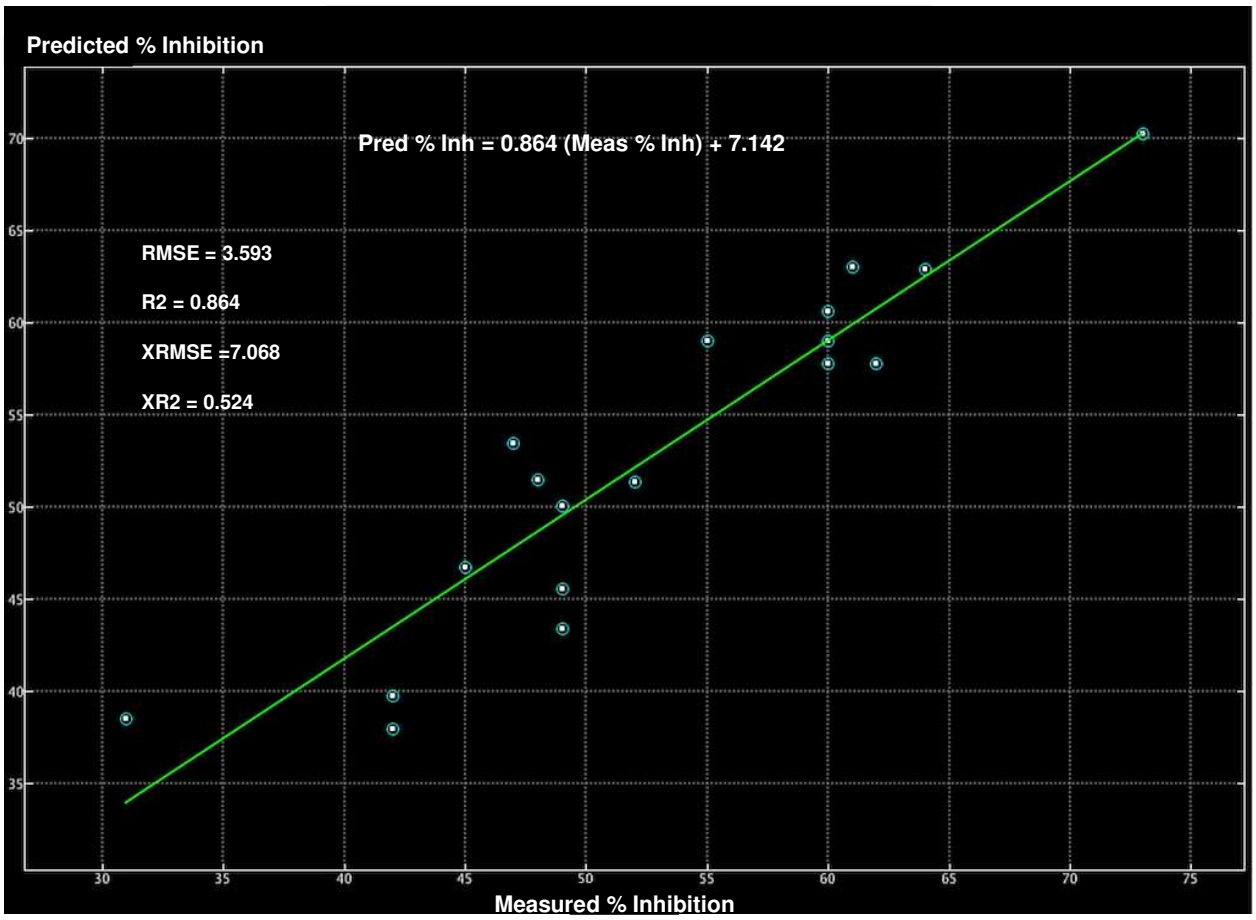

Figure 7: Linear correlation graph comparing a 20 compound training set of measured IC_{50}'s with predicted values based on the calculated 2D QSAR regression model. The linearity of the training set model is shown with the values of the error (RMSE) and correlation factor (R^2) for both validated and cross-validated regressions.

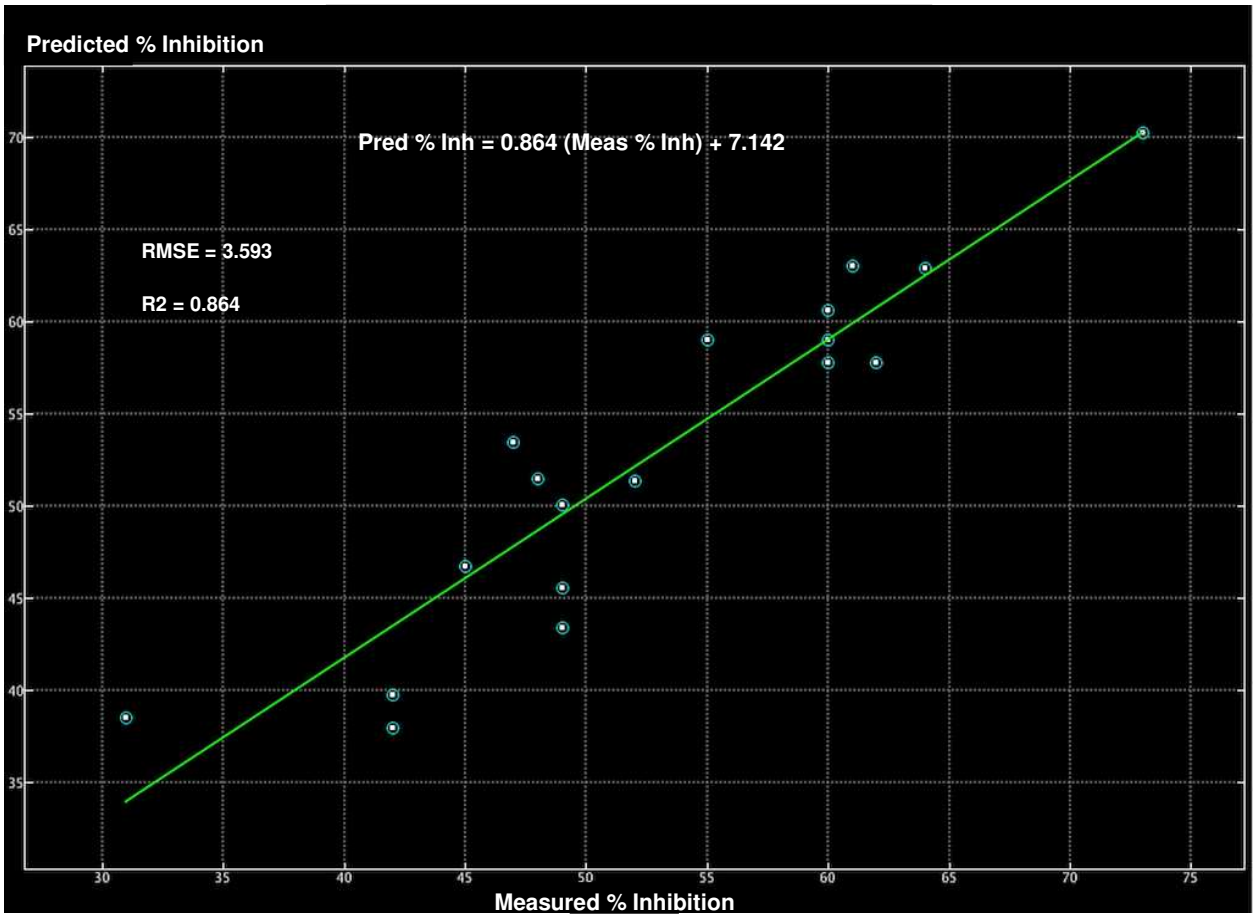

Figure 8: Linear correlation graph comparing a randomly selected 20 compound test set of measured IC50's with predicted values based on the calculated 2D QSAR training set regression model. The linearity of the test model is shown with the values of the error (RMSE) and correlation factor (R^2).

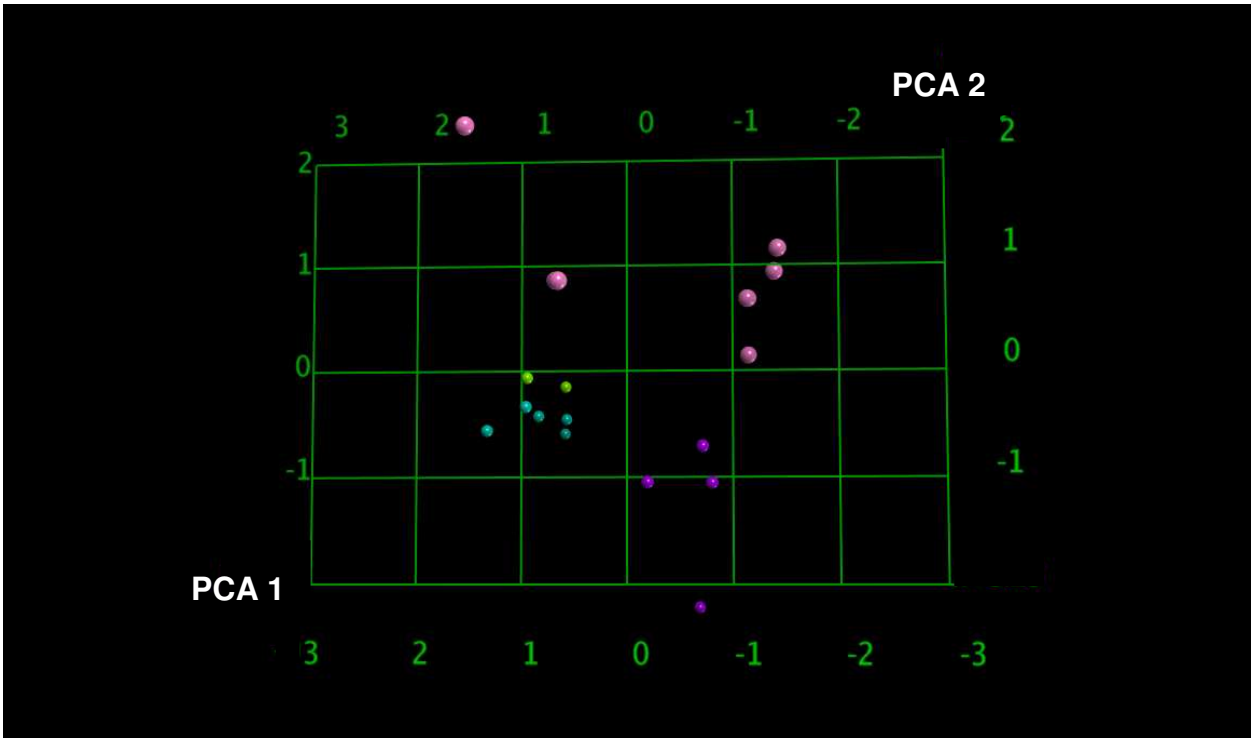

Figure 9: PCA plot of the training set of 20 AChE inhibitor compounds. The first two eigenvectors are shown (PCA 1, PCA 2) projected upon PCA 3, which constituted 100 % of the variance. The spheres indicate the position of each of the compounds within the set with measured activity (% inhibition). Based on VSA,vol, vsa_pol and zagreb descriptors a clear separation between the top 6 active and less active candidates is observed within the region: PCA 1 = -2 to +2, PCA 2 > 0,

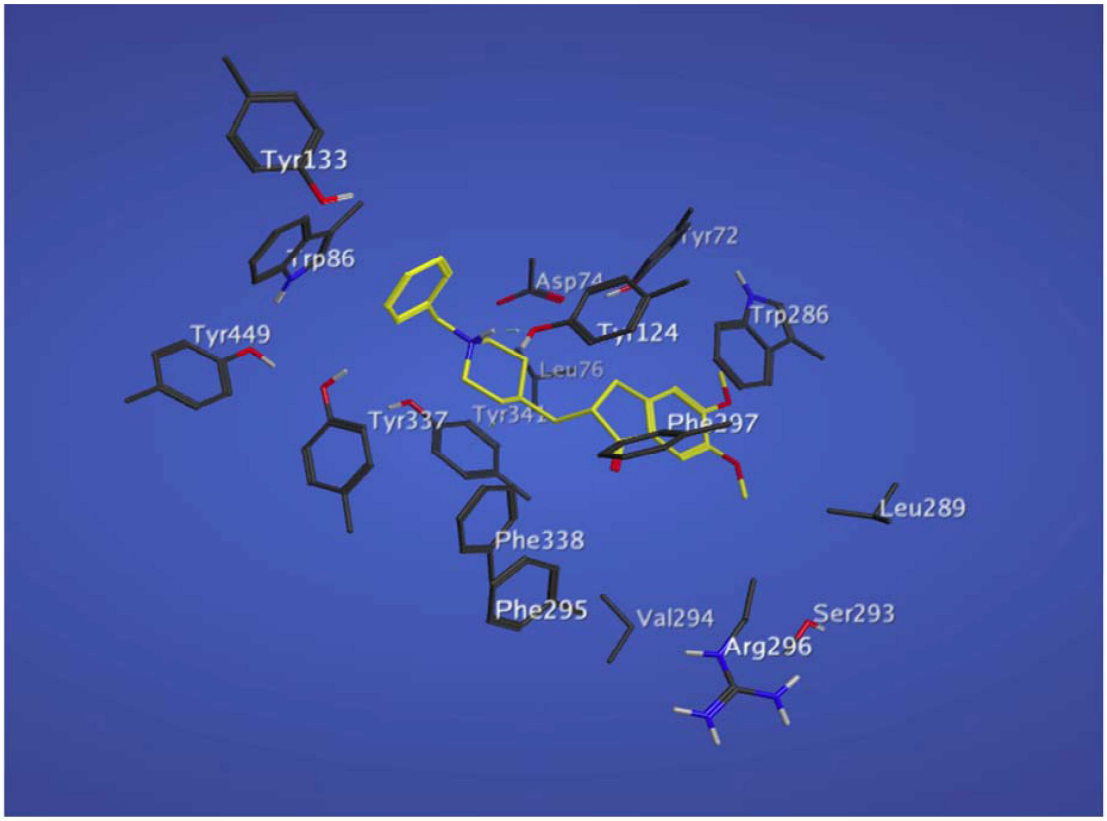

Figure 10. AChE active site for binding of Donepezil is shown in yellow. Residues that contribute to its binding stabilization are indicated.

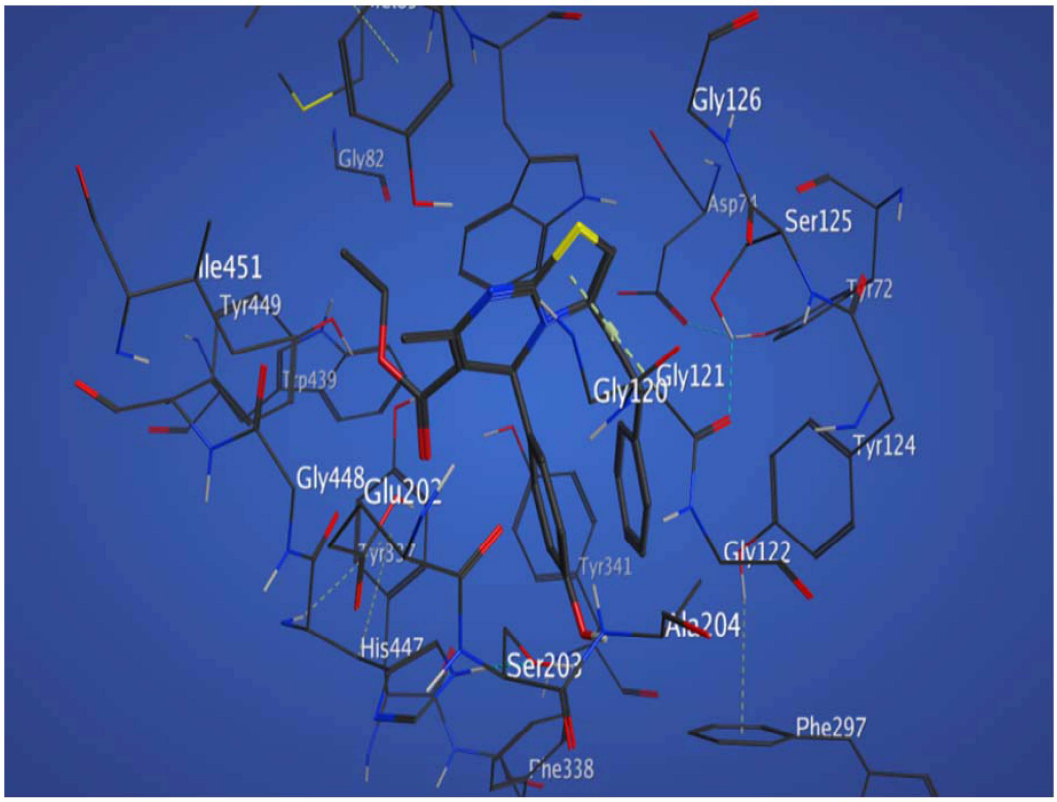

Figure 11. AChE active site for binding of lead candidate (compound **7c**), shown with bold bonds and standard colors for nonhydrogen atoms. Residues that contribute to its binding stabilization are indicated. The binding affinity (GBV!/WSA scoring function) was calculated as -8.6 (+/- 0.3)kcal/mole, and Generalized Born solvation energy as -24.9(+/- 1.0).

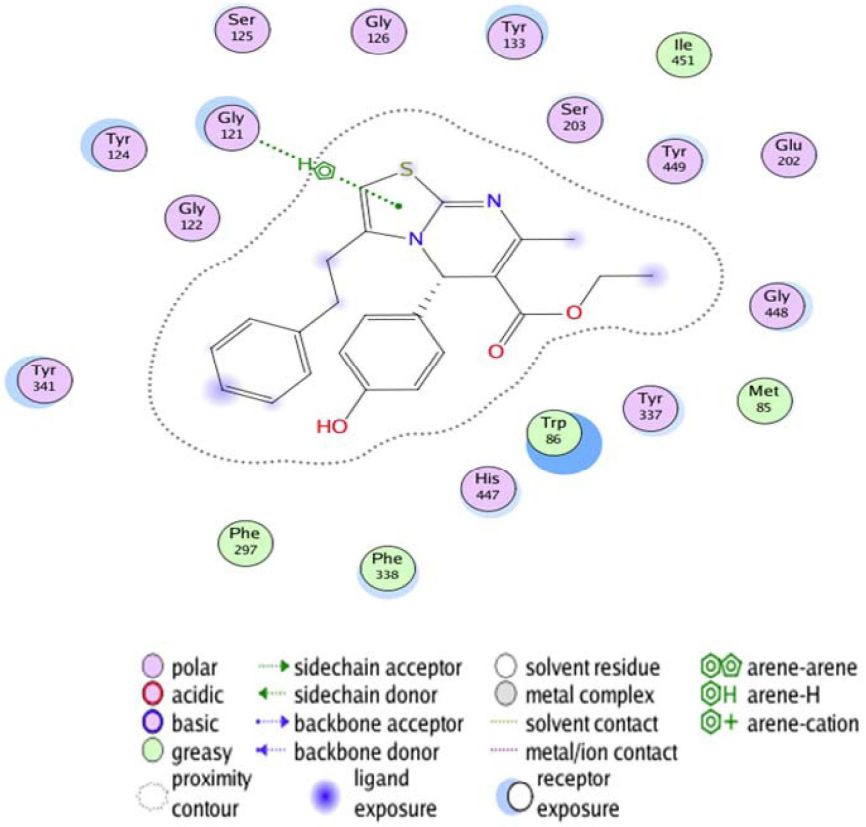

Figure 12. 2D ligand interaction diagram for lead candidate (compound **7c**), showing AChE residues important for binding stabilization. As indicated, arene-H-bonds, aromatic-stacking and hydrophobic interactions play an import role in binding stabilization.

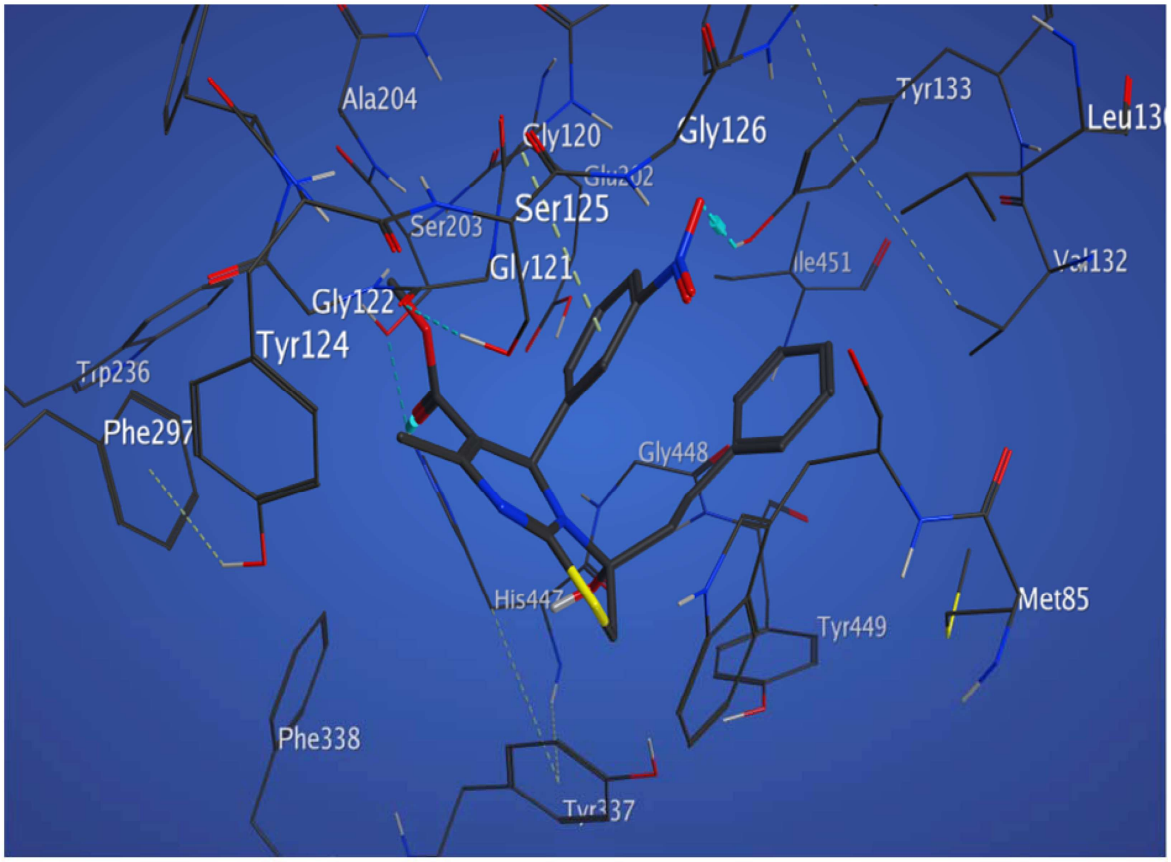

Figure 13. AChE active site for binding of lead candidate (compound **7h**), shown with bold bonds and standard colors for nonhydrogen atoms. Residues that contribute to its binding stabilization are indicated. The binding affinity (GBV!/WSA scoring function) was calculated as -8.3 (+/- 0.3)kcal/mole, and Generalized Born solvation energy as -21.8(+/- 1.0).

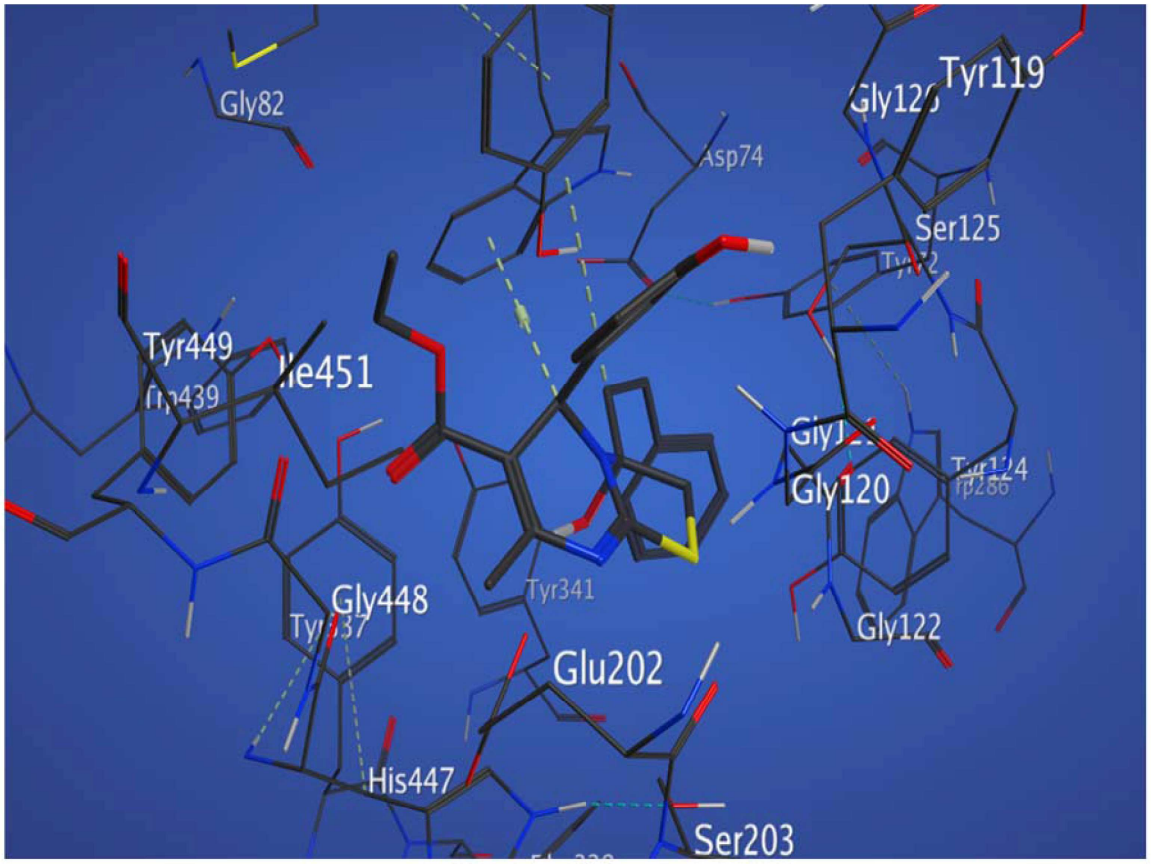

Figure 14. AChE active site for binding of lead candidate (compound **6c**), shown with bold bonds and standard colors for nonhydrogen atoms. Residues that contribute to its binding stabilization are indicated. The binding affinity (GBV!/WSA scoring function) was calculated as -8.3 (+/- 0.3)kcal/mole, and Generalized Born solvation energy as -23.3(+/- 1.0).

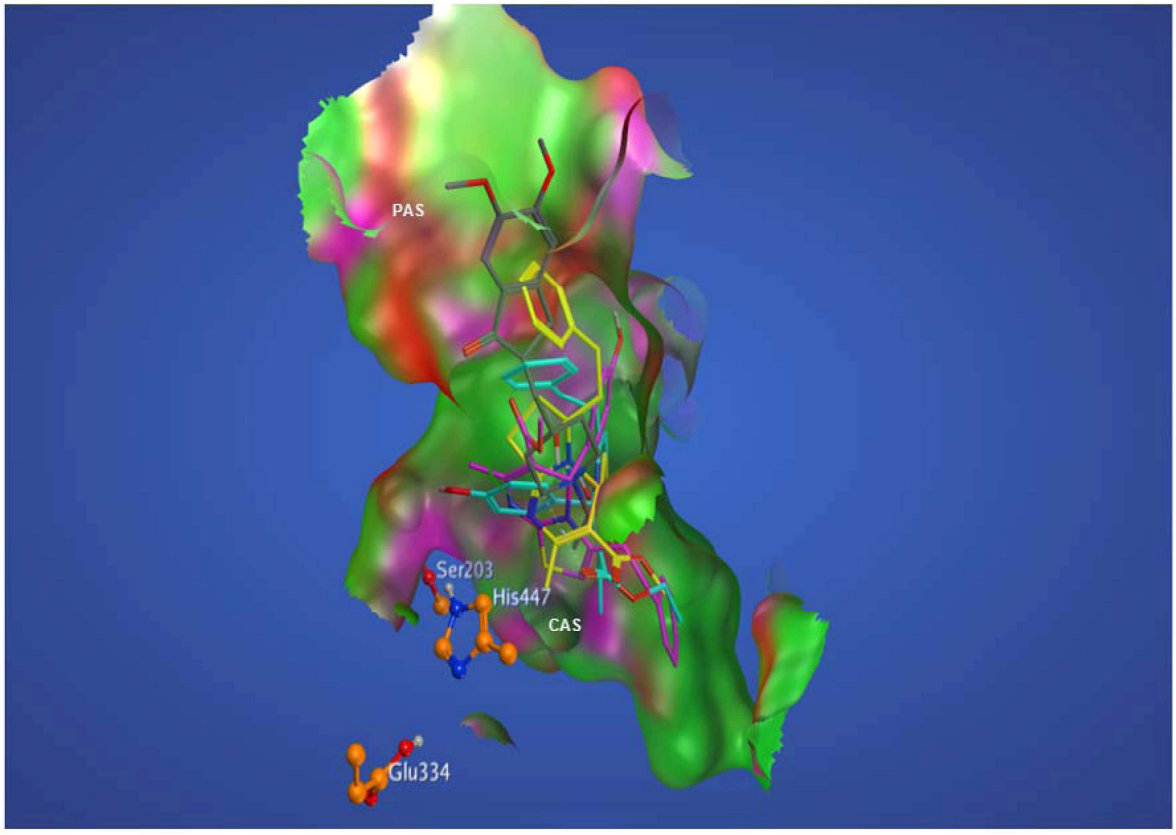

Figure 15. Compounds **Donepezil, 6c**,**7c** and **7h** are shown in their docked position within the 1B41 structure. The peripheral active site (PAS) and catalytic active site (CAS) regions are indicated. The enzymatic triad (S203, H447 and E334) are shown relative to the docked potential candidates. Donepezil is shown in grey, compounds **6c** in yellow, **7c** in turquoise and **7h** in magenta. All are nicely contained within the VDW surface defined by the AChE receptor

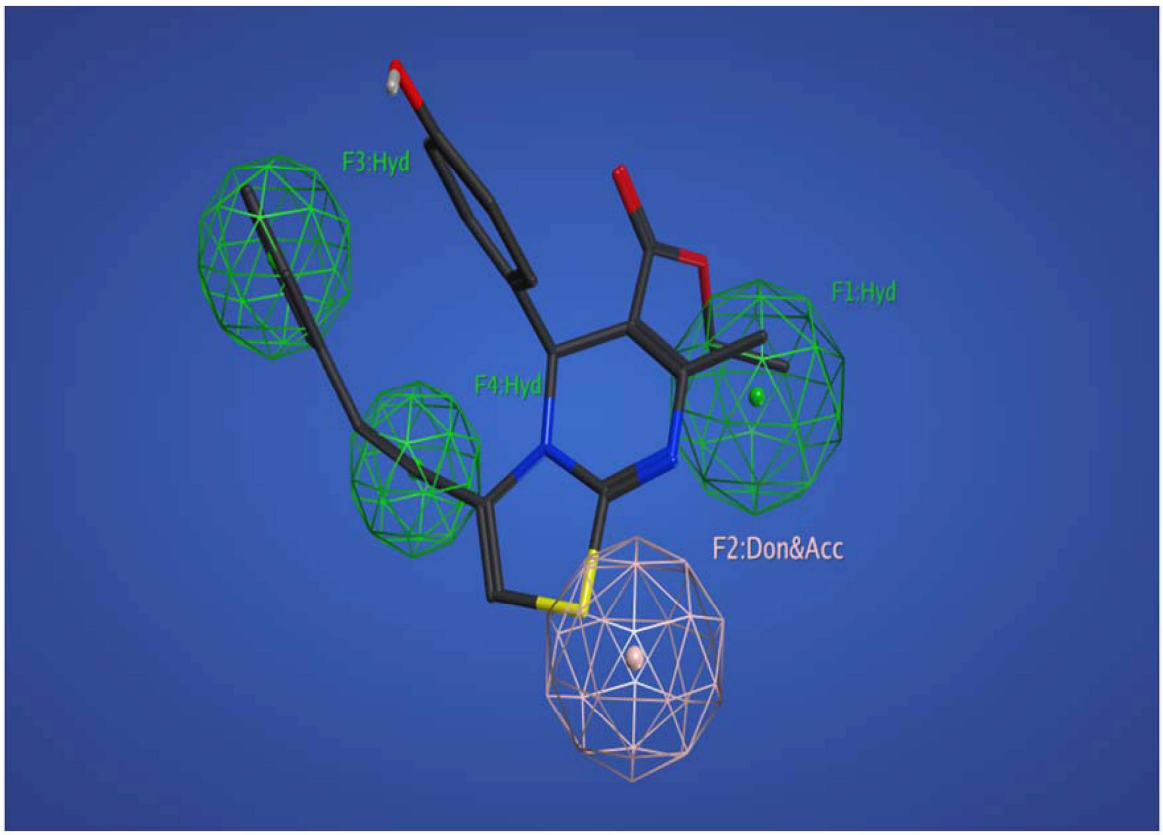

Figure 16. AChE pharmacophore model composed of the hydrophobic regions (Hyd) and H-bond donor/acceptor (Don&Acc). Compound **7c** is shown superimposed as occupying all four regions of the model.

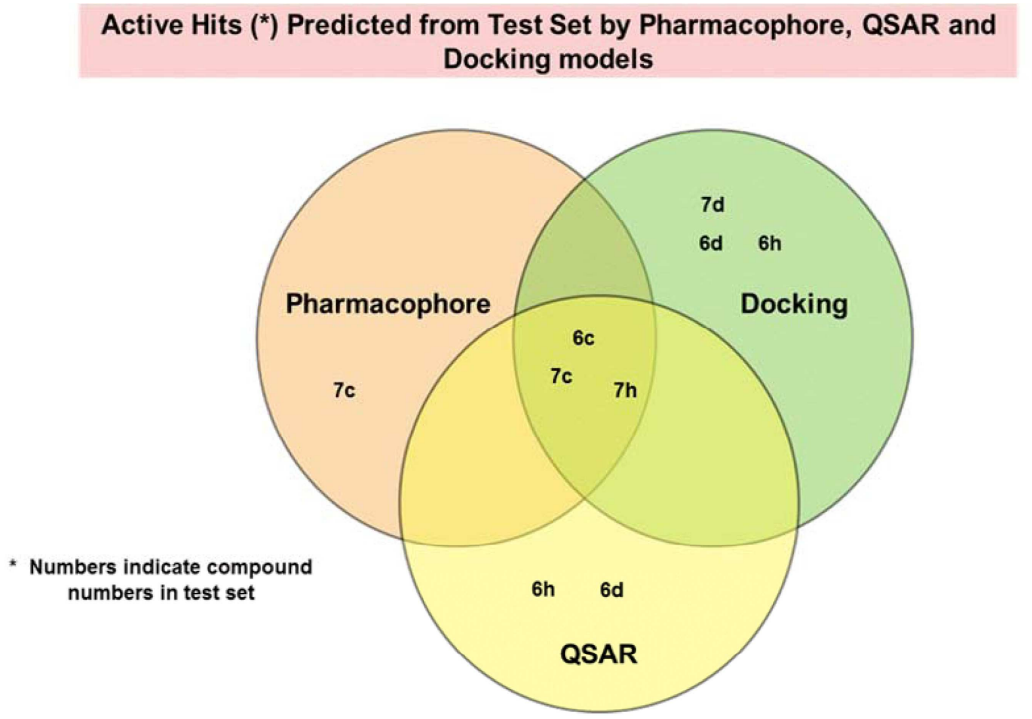

Figure 17. Union of predicted hits by QSAR, pharmacophore and ligand docking with best ligands included in all three circles.

Table 1. Crystal Data and Details of the Structure Determination for **6a & 6e**

Identification code	**6a**	**6e**
Empirical formula	$C_{24}H_{26}BrN_3O_5S$	$C_{26}H_{29}BrN_2O_6S$
Formula weight	548.45	577.48
Temperature	100(2) K	100(2) K
Wavelength	1.54178 Å	1.54178 Å
Crystal system	Monoclinic	Monoclinic
Space group	$P2_1/n$ [an alternate setting of $P2_1/c$ – C_{2h}^5 (No. 14)]	$P2_1/c$
Unit cell dimensions	a = 11.8312(3) Å α= 90.000° b = 14.0673(4) Å β=101.301(1)° c = 14.5827(4) Å γ= 90.000°	a = 17.3323(4) Å α= 90.000° b = 9.4672(3) Å β= 110.0380(10)°. c = 17.1701(4) Å γ = 90.000°
Volume	2380.0(1) $Å^3$	2646.9(1) $Å^3$
Z	4	4
Density (calculated)	1.531 g/cm^3	1.449 gg/cm^3
Absorption coefficient	3.527 mm^{-1}	3.218 mm^{-1}
F(000)	1128	1192
Crystal size	0.12 x 0.11 x 0.06 mm^3	0.08 x 0.03 x 0.03 mm^3
Theta range for data collection	4.41° to 69.76°	2.71° to 70.00°
Index ranges	$-14 \le h \le 14$, $-16 \le k \le 16$, $-17 \le l \le 14$	$-20 \le h \le 20$, $-11 \le k \le 11$, $-20 \le l \le 20$
Reflections collected	22191	23911

Independent reflections	4389 [R_{int} = 0.019]	4887 [R_{int} = 0.041]
Completeness to theta = 66.00°	99.7 %	99.7 %
Absorption correction	Multi-scan	Multi-scan
Max. and min. transmission	1.000 and 0.808	1.000 and 0.881
Refinement method	Full-matrix least-squares on F^2	Full-matrix least-squares on F^2
Data / restraints / parameters	4389 / 0 / 411	4887 / 0 / 441
Goodness-of-fit on F^2	1.102	1.045
Final R indices [I>2sigma(I)]	R_1 = 0.026, wR_2 = 0.068	R_1 = 0.035, wR_2 = 0.085
R indices (all data)	R_1 = 0.026, wR_2 = 0.069	R_1 = 0.038, wR_2 = 0.086
Largest diff. peak and hole	0.48 and -0.30 $e^-/Å^3$	0.82 and -0.50 $e^-/Å^3$

Table 2. Crystal Data and Details of the Structure Determination for **7a** and **7i**

Identification code	**7a**	**7i**
Empirical formula	$C_{24}H_{24}BrN_3O_4S$	$C_{46}H_{46}Br_2N_4O_6S_2$
Formula weight	530.43	974.81
Temperature	100(2) K	100(2) K
Wavelength	1.54178 Å	1.54178 Å
Crystal system	Triclinic	Monoclinic
Space group	$P\bar{1} - C_i^1$ (No. 2)	$P2_1/c$
Unit cell dimensions	a = 6.9449(2) Å α= 63.855(1)°. b = 13.1458(3) Å β= 82.550(1)°. c = 14.5214(4) Å γ = 77.793(1)°.	a = 13.519(2) Å α= 90.000° b = 18.428(3) Å β= 90.674(3)° c = 17.734(3) Å γ = 90.000°
Volume	1162.19(5) $Å^3$	4417.6(12) $Å^3$
Z	2	4
Density (calculated)	1.516 g/cm^3	1.466 Mg/m^3
Absorption coefficient	3.559 mm^{-1}	3.642 mm-1
F(000)	544	2000
Crystal size	0.08 x 0.07 x 0.04 mm^3	0.23 x 0.12 x 0.11 mm^3
Theta range for data collection	3.39° to 69.84°	3.27° to 68.06°
Index ranges	$-8 \le h \le 8, -15 \le k \le 15, -15 \le l \le 17$	$-16 \le h \le 13, -22 \le k \le 21, -21 \le l \le 20$
Reflections collected	10712	28150
Independent	4023 [R_{int} = 0.014]	7814 [R_{int} = 0.022]

reflections		
Completeness to theta = 66.00°	95.2 %	99.2 %
Absorption correction	Multi-scan	Multi-scan
Max. and min. transmission	1.000 and 0.891	1.000 and 0.630
Refinement method	Full-matrix least-squares on F^2	Full-matrix least-squares on F^2
Data / restraints / parameters	4023 / 0 / 394	7814 / 0 / 686
Goodness-of-fit on F^2	1.070	1.076
Final R indices [I>2sigma(I)]	$R_1 = 0.023$, $wR_2 = 0.060$	$R_1 = 0.035$, $wR_2 = 0.094$
R indices (all data)	$R_1 = 0.024$, $wR_2 = 0.060$	$R_1 = 0.035$, $wR_2 = 0.094$
Largest diff. peak and hole	0.54 and -0.29 $e^-/Å^3$	0.69 and -0.55 $e^-/Å^3$

Table 3. Synthesis of tetrahydropyrimidine derivatives

Entry	R^1	R^2	Reaction time (h)	Yield (%)	Melting Points (°C)	
					Observed[a]	Literature[b]
4a	3-NO_2	Ethyl	4	87	204−206	206−207[70]
4b	4- NO_2	Ethyl	5	88	110−111	111−112[71]
4c	4-F	Ethyl	3	92	185−187	186–188[70]
4d	4-OH	Ethyl	4.5	89	199-200	198−200[72]
4e	4-OH,5-$OOCH_3$	Ethyl	8	87	239-240	--
4f	3-NO_2	Methyl	5	92	250−252	249−251[70]
4g	4- NO_2	Methyl	6	94	205−207	204−207[70]
4h	4-F	Methyl	4	91	184−186	183−184[70]
4i	4-OH	Methyl	6	86	210−211	209−212[70]
4j	4-OH,5-$OOCH_3$	Methyl	7	84	211-212	--

[b]All the melting points were matched with the reported data.

Table 4. Definition of Descriptors

vsa_pol	Approximation to the sum of VDW surface areas (Å2) of polar atoms (atoms) that are both hydrogen bond donors and acceptors), such as -OH.
vsa_hyd	Approximation to the sum of VDW surface areas of hydrophobic atoms (Å2).
VSA	van der Waals surface area. A polyhedral representation is used for each atom in calculating the surface area.
zagreb	Zagreb index: the sum of ***d2*** over all heavy atoms *i*.
WeinerPath	Wiener path number: half the sum of all the distance matrix entries as defined in [Balaban 1979] and [Wiener 1947].
WeinerPol	Half the sum of all distance matrix entries with a value of 3
vol	van der Waals volume calculated using a grid approximation (spacing 0.75A).

Table 5. Tabulation of binding affinities and solvation energies for top docking candidates (**6c**, **7c** and **7h**) relative to donepezil.

Compound	Binding Affinity (kcal/mole)	Born Solvation Energy (kcal/mole)
Donepezil	- 8.0 (0.3)	- 28.2 (1.0)
Compound 6c	- 8.3 (0.3)	- 23.3 (1.0)
Compound 7c	- 8.6 (0.3)	- 24.9 (1.0)
Compound 7h	- 8.3 (0.3)	- 21.8 (1.0)

Table 6. Hits Determined by the 4 Feature Pharmacophore Model

	mol	rmsd	mseq	$PRED_HITS	Comp ID
1	Fragment	0.8612	1	-15.2740	6a
2	Fragment	0.7232	2	-8.0505	6b
3	Fragment	0.6036	3	53.2487	6c
4	Fragment	1.0910	4	29.4373	6d
5	Fragment	0.5787	5	-13.5831	6e
6	Fragment	0.8709	6	-32.6843	6f
7	Fragment	0.9098	7	-24.8801	6g
8	Fragment	0.6027	8	36.3966	6h
9	Fragment	0.5879	9	-34.9239	6j
10	Fragment	0.9033	10	59.6933	7c
11	Fragment	0.8815	11	-10.4414	7e
12	Fragment	0.8501	12	44.0813	7h
13	Fragment	0.8418	13	-26.0600	7j

Table 7: ADME properties predicted for 20 novel compounds.

Compound	[a]Human intestinal absorption (%)	[b]*in vitro* Caco-2 cell permeability (nm/sec)	[c]*in vitro* MDCK cell permeability (nm/sec)	[d]*in vitro* plasma protein binding (%)	[e]*in vivo* blood-brain barrier penetration (C.brain/C.blood)
6a	97.561705	19.1355	0.105297	90.484755	0.0806771
6b	97.561705	7.97025	0.105297	90.142982	0.089125
6c	95.389128	31.8492	0.250481	88.226284	0.335066
6d	96.667520	51.638	0.301391	89.418601	0.150767
6e	96.493159	26.3461	0.065936	88.865351	0.0785162
6f	97.176050	19.8794	0.105973	91.276743	0.096315
6g	97.176050	9.71977	0.26827	90.909497	0.198659
6h	95.385717	28.8087	0.239105	88.468882	0.22168
6i	96.676358	49.1567	0.222715	89.696313	0.114523
6j	96.405668	24.6646	0.0872517	89.224416	0.0763619
7a	99.864657	37.971	0.120347	91.316081	0.453354
7b	99.864657	22.9359	0.120347	90.802189	0.487831
7c	96.628366	52.6213	0.407019	89.836610	0.153852
7d	97.487436	57.4001	0.727692	91.158003	0.201717
7e	97.687575	45.3655	0.0596721	89.703433	0.188834
7f	99.796273	35.696	0.102013	91.874991	0.464546
7g	99.796273	22.0079	0.34068	91.304055	0.739628
7h	96.60713	51.3119	0.281396	89.872761	0.140081
7i	97.466478	57.5096	0.380781	91.163376	0.222771
7j	97.820882	41.6557	0.0720615	89.912082	0.230354

[a]Human intestinal absorption is the sum of bioavailability and absorption evaluated from ratio of excretion or cumulative excretion in urine , bile and feces. The value between 0%-20% indicates poor absorption, 20%-70% moderate absorption and 70%-100% well absorption. [b]Caco-2 cells are derived from human colon adenocarcinoma and possess multiple drug transport pathways through the intestinal epithelium. The value <4 indicates low permeability, 4-70 middle permeability and >70 high permeability. [c]MDCK cell system may use as good tool for rapid permeability screening. The value <25 indicates low permeability, 25-500 middle permeability and >500 high permeability. [d]The percent of drug binds to plasma protein. The value <90% indicates weak binding and >90% indicates strong binding to plasma proteins. [e]Blood-Brain Barrier (BBB) penetration is represented as BB = [Brain]/[Blood]. The value <0.1 indicates low absorption, 0.1 – 2.0 middle absorption and >2.0 higher absorption to CNS.

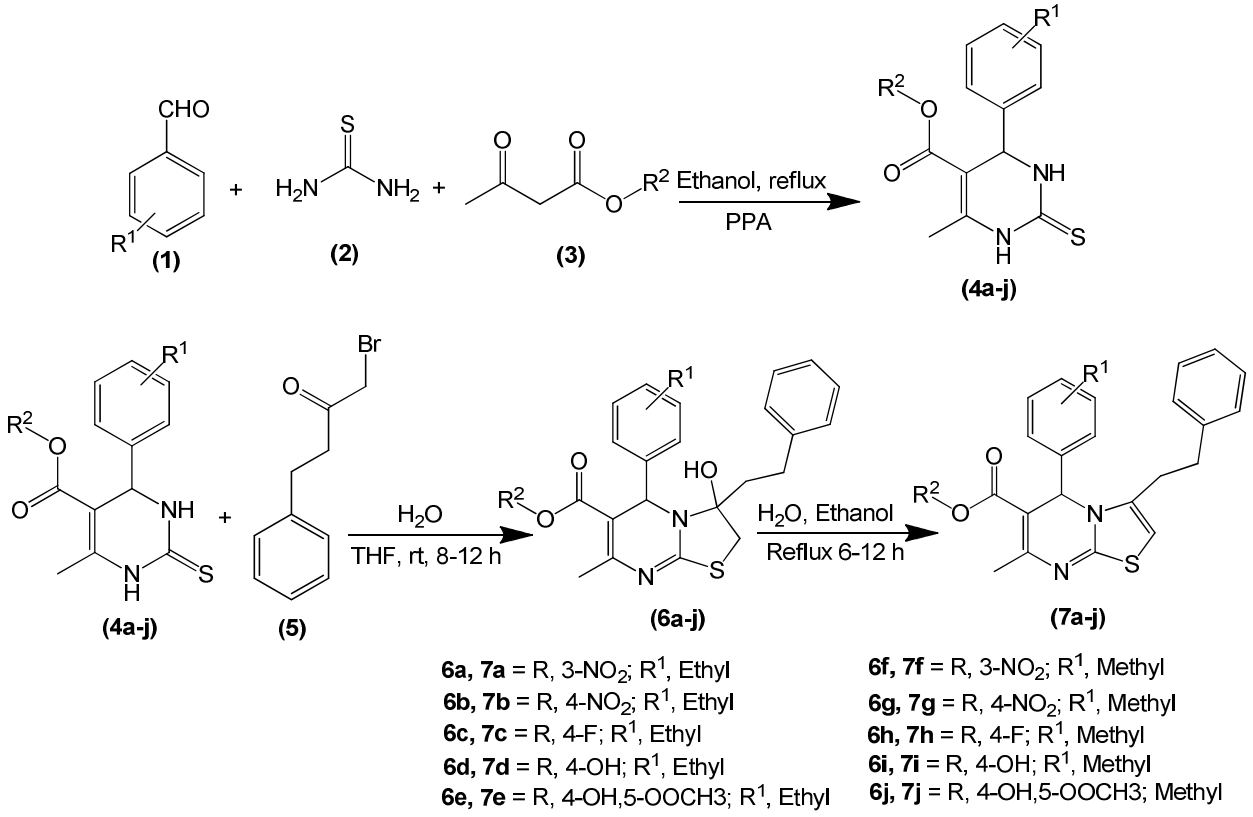

Scheme 1: Representative classes of compounds containing the pyrimidine scaffold and selected molecular targets of Acetylcholinesterase Inhibitors

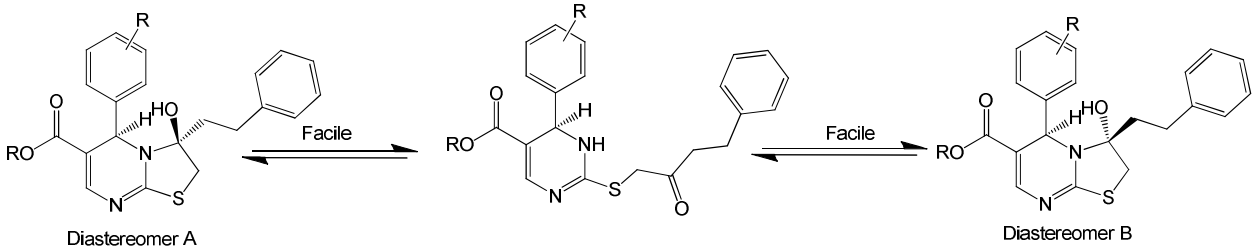

Scheme 2. Diastereomeric representation of compounds **6a-6j**

For Table of Contents Use Only

Acetylcholinesterase Inhibitors: Structure Based Design, Synthesis, Pharmacophore Modeling and Virtual Screening Koteswara Rao Valasani, Michael O. Chaney, Victor W. Day, and Shirley ShiDu Yan